Available online at www.sciencedirect.com
ScienceDirect
Comput. Methods Appl. Mech. Engrg. xxx (xxxx) xxx
Computer methods in applied mechanics and engineering
www.elsevier.com/locate/cma

Large amplitude vibration of FG-CNTRC laminated cylindrical shells with negative Poisson's ratio

Hui-Shen Shen[a,b,*], Chong Li[a], J.N. Reddy[c]

[a] School of Aeronautics and Astronautics, Shanghai Jiao Tong University, Shanghai 200240, People's Republic of China
[b] School of Ocean and Civil Engineering, Shanghai Jiao Tong University, Shanghai 200240, People's Republic of China
[c] Department of Mechanical Engineering, Texas A&M University, College Station, TX 77843-3123, USA

Received 24 June 2019; received in revised form 21 October 2019; accepted 21 October 2019
Available online xxxx

Abstract

This paper presents an investigation on the nonlinear flexural vibrations of carbon nanotube-reinforced composite (CNTRC) laminated cylindrical shells with negative Poisson's ratios in thermal environments. The material properties of the CNTRCs are temperature-dependent and the functionally graded (FG) in a piece-wise pattern in the thickness direction of the shell. An extended Voigt (rule of mixture) model is employed to estimate the CNTRC material properties. The motion equations for the nonlinear flexural vibration of FG-CNTRC laminated cylindrical shells are based on the Reddy's third order shear deformation theory and the von Kármán-type kinematic nonlinearity, and the effects of thermal environmental conditions are included. The nonlinear vibration solutions for the FG-CNTRC laminated cylindrical shells can be obtained by applying a singular perturbation technique along with a two-step perturbation approach. The effects of material property gradient, the temperature variation, shell geometric parameter, stacking sequence as well as the end conditions on the vibration characteristics of CNTRC laminated cylindrical shells are discussed in detail through a parametric study. The results show that negative Poisson's ratio has a significant effect on the linear and nonlinear vibration characteristics of CNTRC laminated cylindrical shells.

Keywords: Nanocomposites; Functionally graded materials; Negative Poisson's ratio; Temperature-dependent properties; Cylindrical shell; Vibration

1. Introduction

Composite laminated shell structures are widely used in structural applications owing to their specific higher strength-to-weight and stiffness-to-weight ratios, improved chemical and environmental resistance and the ability to tailor properties. These shell structures may be exposed to combined action of loading and various environmental conditions during their service life. This may lead to large amplitude vibration of the shells where the shell deflection may be in the order of the shell thickness. In this regard, the nonlinear vibration of composite laminated shells in thermal environments is an important consideration in engineering analysis and design. Many studies have been carried out on the nonlinear vibration behavior of composite laminated shells [1–6]. As pointed out by Shen [6],

* Corresponding author at: School of Aeronautics and Astronautics, Shanghai Jiao Tong University, Shanghai 200240, People's Republic of China.
E-mail address: hsshen@sjtu.edu.cn (H.-S. Shen).

https://doi.org/10.1016/j.cma.2019.112727

Please cite this article as: H.-S. Shen, C. Li and J.N. Reddy, Large amplitude vibration of FG-CNTRC laminated cylindrical shells with negative Poisson's ratio, Computer Methods in Applied Mechanics and Engineering (2019) 112727, https://doi.org/10.1016/j.cma.2019.112727.

unlike in the cases of composite laminated plates, there are unresolved discrepancies between the vibration results obtained by different authors for composite laminated cylindrical shells, in particular for the cases of angle-ply laminated cylindrical shells. With growing interest in the development and manufacturing of high-performance and lightweight composite shells, auxetic composite materials and structures appear to be potential candidates. A consequence of material possessing a negative Poisson's ratio (NPR) is that many of its mechanical properties are predicted to be enhanced by classical elasticity theory. The auxetic materials have a wide variety of multifunctional applications, for example, in energy storage, biomedical, acoustics, photonics, and thermal management [7]. There are two ways to construct auxetic structures. One way is to use auxetic metamaterial as sandwich core [8]. Another way is to change the stacking sequence and orientation of the laminates to obtain auxetic laminated shells. The production of larger values of negative Poisson's ratio requires both a particular stacking sequence and the individual ply material being highly anisotropic [9].

Laminated composite materials made of transversely isotropic laminas may take NPRs due to the configuration of their structures [10]. Herakovich [11] studied the auxetic behavior of angle-ply laminated composites to find the out-of-plane effective Poisson's ratio ν_{13} can range from a high of 0.49 for (90) laminate to a low of -0.21 for a $(\pm 25)_S$ laminate. Lempriere [12] reported that Poisson's ratio in orthotropic materials may be -0.4 when the axes oriented at 45°. Hine et al. [13] reported that the use of a high-modulus carbon fiber can produce an in-plane positive Poisson's ratio of $+2$, and an out-of-plane negative Poisson's ratio of -0.5. Harkati et al. [14] found that negative Poisson's ratio ν_{13} values of up to –0.746 were produced over certain orientation angles for Kevlar and carbon reinforcements. Milton [15] introduced a hybrid composite material made of two different phases with Poisson's ratio approximately equal to -1. Akasaka [16] showed that the out-of-plane Poisson's ratio of a two-ply laminate in excess of –2. Evans et al. [17] showed that a choice of suitable stacking sequences can induce either in-plane or out-of-plane negative Poisson's ratios.

Carbon nanotube reinforced composites (CNTRCs) are a new generation of composite materials in which the ratio of the two in-plane Young's moduli is more than 40 and the in-plane shear modulus is very small in comparison with the longitudinal Young's modulus. Hence, the auxetic CNTRC laminate is expected, and the magnitude of Poisson's ratio may be increased in some directions. Functionally graded materials (FGMs) have emerged as a novel type of composite materials in a wide range of engineering applications [18–23]. Functionally graded carbon nanotube reinforced composites (FG-CNTRCs) were first proposed by Shen [24], and the graded distributions of CNT within an isotropic matrix were designed specifically under certain rules along the desired directions for the purposes of improved structural mechanical properties. The effectiveness of functionally graded reinforcement on the linear and nonlinear vibration capacities of CNTRC cylindrical shells has been further studied by Shen and Xiang [25] and other research teams [26–31].

In the present work, we focus our attention on the nonlinear flexural vibration of CNTRC laminated cylindrical shells with NPR in thermal environments. The novelty of this study lies in the account of both the functionally graded material configurations and the negative Poisson's ratios in the nonlinear vibration analyses of FG-CNTRC laminated cylindrical shells. The out-of-plane NPR is first determined by a particular stacking sequence. The CNT reinforcements are aligned [32] in each layer and the CNTRC layers are arranged in a piece-wise functionally graded pattern along the thickness direction of the shells. The temperature dependent material properties of CNTRC laminates are determined by the extended Voigt (rule of mixture) model in which the CNT efficiency parameters are estimated by matching rule of mixture model results against the elastic moduli of CNTRCs obtained from the molecular dynamics (MD) simulations. The motion equations are based on Reddy's third order shear deformation shell theory with a von Kármán-type of kinematic nonlinearity and include thermal effects. Motion equations are first deduced to a boundary layer type, and a singular perturbation technique in conjunction with a two-step perturbation approach is employed to solve the nonlinear vibration problem.

2. Modeling of FG-CNTRC laminated cylindrical shells with NPR

Consider a laminated cylindrical shell with mean radius R, length L and thickness h which consists of N plies. Each ply is made of a mixture of CNT reinforcement and the isotropic matrix, and may have different value of CNT volume fraction. The CNT reinforcement is aligned in the axial direction and is either uniformly distributed (UD) or functionally graded (FG) in the thickness direction with a piece-wise pattern. As usual, axial, circumferential, and inward through-the-thickness directions of the cylindrical shell are denoted by X, Y, and Z, respectively. The origin of the coordinate system is located at one end of the shell on the middle plane.

Please cite this article as: H.-S. Shen, C. Li and J.N. Reddy, Large amplitude vibration of FG-CNTRC laminated cylindrical shells with negative Poisson's ratio, Computer Methods in Applied Mechanics and Engineering (2019) 112727, https://doi.org/10.1016/j.cma.2019.112727.

In order to conduct piece-wise functionally graded CNTRC laminated shell, we need to select arithmetic series for CNT volume fractions. Three different values 0.11, 0.14 and 0.17 of volume fraction of CNT are evaluated by Han and Elliott [33]. Five different CNT distribution patterns, namely UD, FG-Λ, FG-V, FG-X and FG-O are considered. The CNT volume fractions are gradually increased from inner layer to outer layer in a piece-wise pattern for FG-V type and vice versa for FG-Λ type, the six layer of the two types are denoted by $[0.17_2/0.14_2/0.11_2]$ referred to as FG-V and $[0.11_2/0.14_2/0.17_2]$ referred to as FG-Λ. For FG-O and FG-X distribution types the inner three layers have CNT volume fractions distributed symmetrically with the outer three layers, $[0.11/0.14/0.17]_S$ and $[0.17/0.14/0.11]_S$, referred to as FG-O and FG-X, respectively. For UD distribution type, the CNT volume fraction is distributed uniformly across all layers and in each layer $V_{CN} = 0.14$. Evidently, the two cases of UD and FG CNTRC laminated cylindrical shells will have the same value of total volume fraction of CNT.

2.1. Effective material properties of CNTRC ply

To estimate the effective material properties of the CNTRC laminated cylindrical shell, the extended Voigt model (rule of mixture), in which the CNT efficiency parameters are defined to take the size-dependence of the resulting nanostructures into account, is employed. According to this rule, the effective Young's modulus and shear modulus of each ply can be estimated by [24]

$$E_{11} = \eta_1 V_{CN} E_{11}^{CN} + V_m E^m \tag{1a}$$

$$\frac{\eta_2}{E_{22}} = \frac{V_{CN}}{E_{22}^{CN}} + \frac{V_m}{E^m} \tag{1b}$$

$$\frac{\eta_3}{G_{12}} = \frac{V_{CN}}{G_{12}^{CN}} + \frac{V_m}{G^m} \tag{1c}$$

where E_{11}^{CN}, E_{22}^{CN} and G_{12}^{CN} are the Young's and shear moduli of the CNTs, E^m and G^m are the corresponding properties for the matrix, respectively. V_{CN} and V_m are the volume fractions of the CNT and the matrix, which satisfy the relationship of $V_{CN} + V_m = 1$. Since the reinforcements are in nanoscale, the stress transfer between the matrix and CNTs is not complete. In addition different effects, such as surface effects, strain gradient effects and intermolecular forces are present which are ignored in various conventional micro-mechanics models. Consequently, different micro-mechanical rules such as Voigt model (rule of mixture), Mori–Tanaka model and Halpin–Tsai model cannot be applied directly to estimate the properties of a composite media reinforced with nanofillers. In order to account for the small-scale effect, CNT efficiency parameters η_j $(j = 1, 2, 3)$ are introduced to the original rule of mixture model as given in Eq. (1). The values of η_j are obtained through comparing the results from Eq. (1) against the ones from the MD simulations [33].

The Poisson's ratio and mass density of the composite media may be expressed easily according to the conventional rule of mixture in terms of the Poisson's ratio and mass density of the constituents since it varies in a small range. As a result, Poisson's ratio and mass density of each ply are given by

$$\begin{bmatrix} \nu_{12} \\ \rho \end{bmatrix} = \begin{bmatrix} \nu_{12}^{CN} & \nu^m \\ \rho^{CN} & \rho^m \end{bmatrix} \begin{bmatrix} V_{CN} \\ V_m \end{bmatrix} \tag{2}$$

where ν_{12}^{CN} and ν^m are Poisson's ratios and ρ^{CN} and ρ^m are the mass densities of CNT and matrix, respectively.

Temperature dependent material properties are also considered in the current study. Thermal expansion coefficients of CNTRC layer in the longitudinal and transverse directions are taken according to the Schapery model as [34]

$$\alpha_{11} = \frac{V_{CN} E_{11}^{CN} \alpha_{11}^{CN} + V_m E^m \alpha^m}{V_{CN} E_{11}^{CN} + V_m E^m} \tag{3a}$$

$$\alpha_{22} = (1 + \nu_{12}^{CN}) V_{CN} \alpha_{22}^{CN} + (1 + \nu^m) V_m \alpha^m - \nu_{12} \alpha_{11} \tag{3b}$$

where α_{11}^{CN}, α_{22}^{CN} and α^m are thermal expansion coefficients of CNT and matrix, respectively.

Please cite this article as: H.-S. Shen, C. Li and J.N. Reddy, Large amplitude vibration of FG-CNTRC laminated cylindrical shells with negative Poisson's ratio, Computer Methods in Applied Mechanics and Engineering (2019) 112727, https://doi.org/10.1016/j.cma.2019.112727.

2.2. Effective Poisson's ratios of CNTRC laminated cylindrical shell

For an anisotropic laminated cylindrical shell, the out-of-plane effective Poisson's ratios ν_{13} and ν_{23} can be expressed as

$$\nu_{13}^{e}=-\frac{\begin{vmatrix}\mathbf{A}_{13} & \mathbf{B}_{6\text{-}1}\\ \mathbf{B}_{5\text{-}3} & \mathbf{D}\end{vmatrix}}{\begin{vmatrix}\mathbf{A}_{5\text{-}1} & \mathbf{B}_{6\text{-}1}\\ \mathbf{B}_{5\text{-}1} & \mathbf{D}\end{vmatrix}},\ \nu_{23}^{e}=\frac{\begin{vmatrix}\mathbf{A}_{23} & \mathbf{B}_{6\text{-}2}\\ \mathbf{B}_{5\text{-}3} & \mathbf{D}\end{vmatrix}}{\begin{vmatrix}\mathbf{A}_{5\text{-}2} & \mathbf{B}_{6\text{-}2}\\ \mathbf{B}_{5\text{-}2} & \mathbf{D}\end{vmatrix}} \tag{4}$$

in which

$$\mathbf{A_{13}}=\begin{vmatrix}A_{21}&A_{22}&0&0&A_{26}\\A_{31}&A_{32}&0&0&A_{36}\\0&0&A_{44}&A_{45}&0\\0&0&A_{45}&A_{55}&0\\A_{61}&A_{62}&0&0&A_{66}\end{vmatrix},\quad \mathbf{A_{23}}=\begin{vmatrix}A_{11}&A_{12}&0&0&A_{16}\\A_{31}&A_{32}&0&0&A_{36}\\0&0&A_{44}&A_{45}&0\\0&0&A_{45}&A_{55}&0\\A_{61}&A_{62}&0&0&A_{66}\end{vmatrix},$$

$$\mathbf{A_{5\text{-}1}}=\begin{vmatrix}A_{22}&A_{23}&0&0&A_{26}\\A_{32}&A_{33}&0&0&A_{36}\\0&0&A_{44}&A_{45}&0\\0&0&A_{45}&A_{55}&0\\A_{62}&A_{63}&0&0&A_{66}\end{vmatrix},\quad \mathbf{A_{5\text{-}2}}=\begin{vmatrix}A_{11}&A_{13}&0&0&A_{16}\\A_{31}&A_{33}&0&0&A_{36}\\0&0&A_{44}&A_{45}&0\\0&0&A_{45}&A_{55}&0\\A_{61}&A_{63}&0&0&A_{66}\end{vmatrix},$$

$$\mathbf{B_{5\text{-}1}}=\begin{vmatrix}B_{12}&B_{13}&0&0&B_{16}\\B_{22}&B_{23}&0&0&B_{26}\\B_{32}&B_{33}&0&0&B_{36}\\0&0&B_{44}&B_{45}&0\\0&0&B_{45}&B_{55}&0\\B_{62}&B_{63}&0&0&B_{66}\end{vmatrix},\quad \mathbf{B_{5\text{-}2}}=\begin{vmatrix}B_{11}&B_{13}&0&0&B_{16}\\B_{21}&B_{23}&0&0&B_{26}\\B_{31}&B_{33}&0&0&B_{36}\\0&0&B_{44}&B_{45}&0\\0&0&B_{45}&B_{55}&0\\B_{61}&B_{63}&0&0&B_{66}\end{vmatrix},$$

$$\mathbf{B_{5\text{-}3}}=\begin{vmatrix}B_{11}&B_{12}&0&0&B_{16}\\B_{21}&B_{22}&0&0&B_{26}\\B_{31}&B_{32}&0&0&B_{36}\\0&0&B_{44}&B_{45}&0\\0&0&B_{45}&B_{55}&0\\B_{61}&B_{62}&0&0&B_{66}\end{vmatrix},$$

$$\mathbf{B_{6\text{-}1}}=\begin{vmatrix}B_{21}&B_{22}&B_{23}&0&0&B_{26}\\B_{31}&B_{32}&B_{33}&0&0&B_{36}\\0&0&0&B_{44}&B_{45}&0\\0&0&0&B_{45}&B_{55}&0\\B_{61}&B_{62}&B_{63}&0&0&B_{66}\end{vmatrix},\quad \mathbf{B_{6\text{-}2}}=\begin{vmatrix}B_{11}&B_{12}&B_{13}&0&0&B_{16}\\B_{31}&B_{32}&B_{33}&0&0&B_{36}\\0&0&0&B_{44}&B_{45}&0\\0&0&0&B_{45}&B_{55}&0\\B_{61}&B_{62}&B_{63}&0&0&B_{66}\end{vmatrix},$$

$$\mathbf{D}=\begin{vmatrix}D_{11}&D_{12}&D_{13}&0&0&D_{16}\\D_{21}&D_{22}&D_{23}&0&0&D_{26}\\D_{31}&D_{32}&D_{33}&0&0&D_{36}\\0&0&0&D_{44}&D_{45}&0\\0&0&0&D_{45}&D_{55}&0\\D_{61}&D_{62}&D_{63}&0&0&D_{66}\end{vmatrix}, \tag{5}$$

where A_{ij}, B_{ij}, D_{ij} are the shell stiffnesses, defined by

$$(A_{ij},B_{ij},D_{ij})=\sum_{k=1}^{N}\int_{h_{k-1}}^{h_k}(\bar{C}_{ij})_k(1,Z,Z^2)\mathrm{d}Z\quad (i,j=1\sim6) \tag{6}$$

in which $\bar{C}_{ij}$ are the transformed stiffness coefficients, and

$$[\bar{C}_{ij}]^{-1}=[\bar{S}_{ij}] \tag{7}$$

Please cite this article as: H.-S. Shen, C. Li and J.N. Reddy, Large amplitude vibration of FG-CNTRC laminated cylindrical shells with negative Poisson's ratio, Computer Methods in Applied Mechanics and Engineering (2019) 112727, https://doi.org/10.1016/j.cma.2019.112727.

where $\bar{S}_{ij}$ are the transformed flexibility coefficients, and the details of which may be expressed by

$$\begin{aligned}
\bar{S}_{11} &= S_{11}c^4 + 2(S_{12} + 2S_{66})c^2s^2 + S_{22}s^4,\\
\bar{S}_{12} &= (S_{11} + S_{22} - 4S_{66})c^2s^2 + S_{12}(c^4 + s^4),\\
\bar{S}_{13} &= S_{13}c^2 + S_{23}s^2,\\
\bar{S}_{16} &= (2(S_{11} - S_{12}) - S_{66})c^3s + (2(S_{11} - S_{22}) + S_{66})cs^3,\\
\bar{S}_{22} &= S_{22}c^4 + 2(S_{12} + 2S_{66})c^2s^2 + S_{11}s^4,\\
\bar{S}_{23} &= S_{23}c^2 + S_{13}s^2,\\
\bar{S}_{26} &= (2(S_{11} - S_{12}) - S_{66})cs^3 + (2(S_{11} - S_{22}) + S_{66})c^3s,\\
\bar{S}_{36} &= 2(S_{13} - S_{23})cs,\\
\bar{S}_{44} &= S_{44}c^2 + S_{55}s^2,\\
\bar{S}_{45} &= (S_{55} - S_{44})cs,\\
\bar{S}_{55} &= S_{55}c^2 + S_{44}s^2,\\
\bar{S}_{66} &= 2(2(S_{11} + S_{22} - 2S_{12}) - S_{66})c^2s^2 + S_{66}(s^4 + c^4),
\end{aligned} \tag{8}$$

where S_{ij} are the flexibility coefficients, defined by

$$\begin{aligned}
&S_{11} = \frac{1}{E_{11}}, \quad S_{12} = -\frac{\nu_{12}}{E_{11}}, \quad S_{13} = -\frac{\nu_{13}}{E_{11}}, \quad S_{22} = \frac{1}{E_{22}}, \quad S_{23} = -\frac{\nu_{23}}{E_{22}}, \quad S_{33} = \frac{1}{E_{11}},\\
&S_{44} = \frac{1}{G_{23}}, \quad S_{55} = \frac{1}{G_{13}}, \quad S_{66} = \frac{1}{G_{12}},
\end{aligned} \tag{9}$$

and

$$c = \cos\theta, \qquad s = \sin\theta \tag{10}$$

where E_{11}, E_{22}, G_{12}, G_{13}, G_{23}, ν_{12}, ν_{13} and ν_{23} are Young's moduli, shear moduli, and the Poisson's ratios of the laminate, and θ is the lamination angle with respect to the shell X-axis.

2.3. Motion equations of CNTRC laminated cylindrical shell

The shell is exposed to elevated temperature and is subjected to a transverse dynamic load $q(X, Y, \bar{t})$. Based on Reddy's third order shear deformation theory [35] with a von Kármán-type of kinematic nonlinearity and including thermal effects, the motion equations for CNTRC laminated cylindrical shells can be expressed as

$$\begin{aligned}
&\tilde{L}_{11}(\bar{W}) - \tilde{L}_{12}(\bar{\Psi}_x) - \tilde{L}_{13}(\bar{\Psi}_y) + \tilde{L}_{14}(\bar{F}) - \tilde{L}_{15}(\bar{N}^T) - \tilde{L}_{16}(\bar{M}^T) - \frac{1}{R}\bar{F}_{,XX}\\
&= \tilde{L}(\bar{W}, \bar{F}) + \tilde{L}_{17}(\ddot{\bar{W}}) - \left(\tilde{I}_5\frac{\partial\ddot{\bar{\Psi}}_x}{\partial X} + \tilde{I}_5'\frac{\partial\ddot{\bar{\Psi}}_y}{\partial Y}\right) + q
\end{aligned} \tag{11}$$

$$\tilde{L}_{21}(\bar{F}) + \tilde{L}_{22}(\bar{\Psi}_x) + \tilde{L}_{23}(\bar{\Psi}_y) - \tilde{L}_{24}(\bar{W}) - \tilde{L}_{25}(\bar{N}^T) + \frac{1}{R}\bar{W}_{,XX} = -\frac{1}{2}\tilde{L}(\bar{W}, \bar{W}) \tag{12}$$

$$\tilde{L}_{31}(\bar{W}) + \tilde{L}_{32}(\bar{\Psi}_x) + \tilde{L}_{33}(\bar{\Psi}_y) + \tilde{L}_{34}(\bar{F}) - \tilde{L}_{35}(\bar{N}^T) - \tilde{L}_{36}(\bar{S}^T) = \hat{I}_5\frac{\partial\ddot{\bar{W}}}{\partial X} - \hat{I}_3\ddot{\bar{\Psi}}_x \tag{13}$$

$$\tilde{L}_{41}(\bar{W}) + \tilde{L}_{42}(\bar{\Psi}_x) + \tilde{L}_{43}(\bar{\Psi}_y) + \tilde{L}_{44}(\bar{F}) - \tilde{L}_{45}(\bar{N}^T) - \tilde{L}_{46}(\bar{S}^T) = \hat{I}_5'\frac{\partial\ddot{\bar{W}}}{\partial Y} - \hat{I}_3'\ddot{\bar{\Psi}}_y \tag{14}$$

in which

$$\tilde{L}_{17}() = -I_1 - \left(\tilde{I}_7\frac{\partial^2}{\partial X^2} + \tilde{I}_7'\frac{\partial^2}{\partial Y^2}\right) \tag{15}$$

where a comma denotes partial differentiation with respect to the corresponding coordinates, and $\bar{W}$ is the transverse displacement, $\bar{\Psi}_x$ and $\bar{\Psi}_y$ are the rotations of the normals to the middle surface with respect to the Y - and

Please cite this article as: H.-S. Shen, C. Li and J.N. Reddy, Large amplitude vibration of FG-CNTRC laminated cylindrical shells with negative Poisson's ratio, Computer Methods in Applied Mechanics and Engineering (2019) 112727, https://doi.org/10.1016/j.cma.2019.112727.

X - axes, $\bar{F}$ is the stress function defined by $\bar{N}_x = \partial^2\bar{F}/\partial Y^2$, $\bar{N}_y = \partial^2\bar{F}/\partial X^2$ and $\bar{N}_{xy} = -\partial^2\bar{F}/\partial X\partial Y$. $\tilde{L}_{ij}(\ )$ and $\tilde{L}(\ )$ are linear and nonlinear operators as defined in Shen [36], and $\tilde{L}(\ )$ contains the geometric nonlinearity terms in the von Kármán sense, and can be given by

$$\tilde{L}(\ ) = \frac{\partial^2}{\partial X^2}\frac{\partial^2}{\partial Y^2} - 2\frac{\partial^2}{\partial X\partial Y}\frac{\partial^2}{\partial X\partial Y} + \frac{\partial^2}{\partial Y^2}\frac{\partial^2}{\partial X^2} \tag{16}$$

The shell is assumed to be in a constant temperature field at an isothermal state. The terms associated with the superscript T in Eqs. (11)–(14) contain the effect of temperature variation, $\bar{N}^T$ are the thermal forces, $\bar{M}^T$ are the thermal moments and $\bar{P}^T$ are the higher order thermal moments. The superposed dots are differentiation with respect to time and the inertias I_j, $\hat{I}_j$ and $\tilde{I}_j$ as well as $\bar{N}^T$, $\bar{M}^T$ and $\bar{P}^T$ are given in detail in Appendix A.

The two end edges of the shell are assumed to be simply supported or clamped, and with or without longitudinal displacements, referred to as 'movable' and 'immovable' in the following, when temperature is increased steadily, so that the boundary conditions are

$X = 0, L$:

$$\bar{W} = \bar{V} = \bar{\Psi}_y = 0, \qquad \bar{M}_x = \bar{P}_x = 0 \quad \text{(simply supported)} \tag{17a}$$

$$\bar{W} = \bar{V} = \bar{\Psi}_x = \bar{\Psi}_y = 0 \quad \text{(clamped)} \tag{17b}$$

where $\bar{V}$ is the displacement in the Y-direction, and $\bar{M}_x$ is the bending moment and $\bar{P}_x$ is the higher order moment, as defined in Reddy and Liu [35].

For immovable in-plane boundary conditions, one has

$$\bar{U} = 0 \quad (at\ X = 0, L) \tag{18}$$

where $\bar{U}$ is the displacement in the X-direction. The conditions expressing the immovability condition (18) may be fulfilled on the average sense as

$$\int_0^{2\pi R}\int_0^L \frac{\partial\bar{U}}{\partial X}dXdY = 0 \tag{19a}$$

or

$$\begin{aligned}\int_0^{2\pi R}\int_0^L \Bigg[&\left(A_{11}^*\frac{\partial^2\bar{F}}{\partial Y^2} + A_{12}^*\frac{\partial^2\bar{F}}{\partial X^2} - A_{16}^*\frac{\partial^2\bar{F}}{\partial X\partial Y}\right) + \left(B_{11}^* - \frac{4}{3h^2}E_{11}^*\right)\frac{\partial\bar{\Psi}_x}{\partial X}\\ &+ \left(B_{12}^* - \frac{4}{3h^2}E_{12}^*\right)\frac{\partial\bar{\Psi}_y}{\partial Y} + \left(B_{16}^* - \frac{4}{3h^2}E_{16}^*\right)\left(\frac{\partial\bar{\Psi}_x}{\partial Y} + \frac{\partial\bar{\Psi}_y}{\partial X}\right)\\ &- \frac{4}{3h^2}\left(E_{11}^*\frac{\partial^2\bar{W}}{\partial X^2} + E_{12}^*\frac{\partial^2\bar{W}}{\partial Y^2} + 2E_{16}^*\frac{\partial^2\bar{W}}{\partial X\partial Y}\right)\\ &- \frac{1}{2}\left(\frac{\partial\bar{W}}{\partial X}\right)^2 - (A_{11}^*\bar{N}_x^T + A_{12}^*\bar{N}_y^T + A_{16}^*\bar{N}_{xy}^T)\Bigg]dXdY = 0\end{aligned} \tag{19b}$$

Also, we have periodicity (or closed) condition

$$\int_0^{2\pi R}\frac{\partial\bar{V}}{\partial Y}dY = 0 \tag{20a}$$

or

$$\begin{aligned}\int_0^{2\pi R}\Bigg[&\left(A_{22}^*\frac{\partial^2\bar{F}}{\partial X^2} + A_{12}^*\frac{\partial^2\bar{F}}{\partial Y^2} - A_{26}^*\frac{\partial^2\bar{F}}{\partial X\partial Y}\right) + \left(B_{21}^* - \frac{4}{3h^2}E_{21}^*\right)\frac{\partial\bar{\Psi}_x}{\partial X} + \left(B_{22}^* - \frac{4}{3h^2}E_{22}^*\right)\frac{\partial\bar{\Psi}_y}{\partial Y}\\ &+ \left(B_{26}^* - \frac{4}{3h^2}E_{26}^*\right)\left(\frac{\partial\bar{\Psi}_x}{\partial Y} + \frac{\partial\bar{\Psi}_y}{\partial X}\right) - \frac{4}{3h^2}\left(E_{21}^*\frac{\partial^2\bar{W}}{\partial X^2} + E_{22}^*\frac{\partial^2\bar{W}}{\partial Y^2} + 2E_{26}^*\frac{\partial^2\bar{W}}{\partial X\partial Y}\right)\\ &+ \frac{\bar{W}}{R} - \frac{1}{2}\left(\frac{\partial\bar{W}}{\partial Y}\right)^2 - (A_{12}^*\bar{N}_x^T + A_{22}^*\bar{N}_y^T + A_{26}^*\bar{N}_{xy}^T)\Bigg]dY = 0\end{aligned} \tag{20b}$$

Please cite this article as: H.-S. Shen, C. Li and J.N. Reddy, Large amplitude vibration of FG-CNTRC laminated cylindrical shells with negative Poisson's ratio, Computer Methods in Applied Mechanics and Engineering (2019) 112727, https://doi.org/10.1016/j.cma.2019.112727.

Note that both the periodicity condition of Eq. (20) and the in-plane boundary condition $\bar{V}=0$ (at $X=0, L$) achieve the same effect. Hence, $\bar{V}=0$ in Eqs. (17a) and (17b) may be neglected when Eq. (20) is applied.

In the above equations, the reduced stiffness matrices $[A^*_{ij}]$, $[B^*_{ij}]$, $[D^*_{ij}]$, $[E^*_{ij}]$, $[F^*_{ij}]$ and $[H^*_{ij}]$ are defined in Appendix B.

3. Solution procedure

The boundary layer phenomenon was previously observed in the nonlinear vibration of anisotropic laminated cylindrical shells [6]. In order to account for the boundary layer effect in the nonlinear vibration analysis of CNTRC laminated cylindrical shells, the motion equations (11)–(14) are first deduced to the non-dimensional forms as

$$\begin{aligned}&\varepsilon^2 L_{11}(W)-\varepsilon L_{12}(\Psi_x)-\varepsilon L_{13}(\Psi_y)+\varepsilon\gamma_{14}L_{14}(F)-\varepsilon L_{16}(M^T)-\gamma_{14}F_{,xx}\\&=\gamma_{14}\beta^2 L(W,F)+\varepsilon^2 L_{17}(\ddot{W})+\varepsilon\left(\gamma_{81}\frac{\partial\ddot{\Psi}_x}{\partial x}+\gamma_{82}\beta\frac{\partial\ddot{\Psi}_y}{\partial y}\right)+\gamma_{14}\frac{4}{3}(3)^{1/4}\lambda_q\varepsilon^{3/2}\end{aligned}\tag{21}$$

$$L_{21}(F)+\gamma_{24}L_{22}(\Psi_x)+\gamma_{24}L_{23}(\Psi_y)-\varepsilon\gamma_{24}L_{24}(W)+\gamma_{24}W_{,xx}=-\frac{1}{2}\gamma_{24}\beta^2 L(W,\ W)\tag{22}$$

$$\varepsilon\, L_{31}(W)+L_{32}(\Psi_x)+L_{33}(\Psi_y)+\gamma_{14}L_{34}(F)-L_{36}(S^T)=\varepsilon\,\gamma_{83}\frac{\partial\ddot{W}}{\partial x}+\gamma_{91}\ddot{\Psi}_x\tag{23}$$

$$\varepsilon\, L_{41}(W)+L_{42}(\Psi_x)+L_{43}(\Psi_y)+\gamma_{14}L_{44}(F)-L_{46}(S^T)=\varepsilon\,\gamma_{84}\beta\frac{\partial\ddot{W}}{\partial y}+\gamma_{92}\ddot{\Psi}_y\tag{24}$$

where

$$L_{17}(\quad)=\gamma_{170}+\left(\gamma_{171}\frac{\partial^2}{\partial x^2}+\gamma_{172}\beta^2\frac{\partial^2}{\partial y^2}\right)\tag{25}$$

where the dimensionless operators $L_{ij}(\ )$ and $L(\ )$ are defined as in Shen [36]. In these equations, the non-dimensional parameters are defined by

$$\begin{aligned}&x=\pi\frac{X}{L},\ y=\frac{Y}{R},\ \beta=\frac{L}{\pi R},\ \bar{Z}=\frac{L^2}{Rh},\ \varepsilon=\frac{\pi^2 R}{L^2}[D^*_{11}D^*_{22}A^*_{11}A^*_{22}]^{1/4},\\&W=\varepsilon\frac{\bar{W}}{[D^*_{11}D^*_{22}A^*_{11}A^*_{22}]^{1/4}},\ F=\varepsilon^2\frac{\bar{F}}{[D^*_{11}D^*_{22}]^{1/2}},\ (\Psi_x,\ \Psi_y)=\varepsilon^2\frac{L}{\pi}\frac{(\bar{\Psi}_x,\ \bar{\Psi}_y)}{[D^*_{11}D^*_{22}A^*_{11}A^*_{22}]^{1/4}},\\&(M_x,\ P_x)=\varepsilon^2\frac{L^2}{\pi^2}\frac{1}{D^*_{11}[D^*_{11}D^*_{22}A^*_{11}A^*_{22}]^{1/4}}\left(\bar{M}_x,\ \frac{4}{3h^2}\bar{P}_x\right),\ \omega_L=\Omega_L\frac{L}{\pi}\sqrt{\frac{\rho_0}{E_0}},\ t=\frac{\pi\,\bar{t}}{L}\sqrt{\frac{E_0}{\rho_0}},\\&\lambda_q=\frac{q(3)^{3/4}LR^{3/2}}{4\pi}\frac{(A^*_{11}A^*_{22})^{1/8}}{(D^*_{11}D^*_{22})^{3/8}},\ \gamma_{14}=\left[\frac{D^*_{22}}{D^*_{11}}\right]^{1/2},\ \gamma_{24}=\left[\frac{A^*_{11}}{A^*_{22}}\right]^{1/2},\ \gamma_5=-\frac{A^*_{12}}{A^*_{22}},\\&(\gamma_{T1},\ \gamma_{T2},\ \gamma_{T3})=(A^T_x,\ A^T_y,\ A^T_{xy})R\left[\frac{A^*_{11}A^*_{22}}{D^*_{11}D^*_{22}}\right]^{1/4},\ \gamma_{170}=-\frac{I_1E_0L^2}{\pi^2\rho_0D^*_{11}},\\&(\gamma_{T4},\gamma_{T5},\gamma_{T6},\gamma_{T7},\ \gamma_{T8},\ \gamma_{T9})=\frac{L^2}{\pi^2hD^*_{11}}(D^T_x,\ D^T_y,\ D^T_{xy},\ \frac{4}{3h^2}F^T_x,\ \frac{4}{3h^2}F^T_y,\frac{4}{3h^2}F^T_{xy}),\\&(\gamma_{91},\ \gamma_{92},\gamma_{81},\ \gamma_{82},\ \gamma_{83},\ \gamma_{84},\ \gamma_{171},\gamma_{172})=(-\hat{I}_3,\ -\hat{I}'_3,\ -\tilde{I}_5,\ -\tilde{I}'_5,\ \hat{I}_5,\ \hat{I}'_5,\ -\tilde{I}_7,\ -\tilde{I}'_7)\frac{E_0}{\rho_0D^*_{11}},\end{aligned}\tag{26}$$

in which ρ_0 and E_0 are the reference values of ρ^m and E^m at the room temperature, and A^T_x, A^T_y, etc. are defined by

$$\begin{bmatrix}A^T_x & D^T_x & F^T_x\\ A^T_y & D^T_y & F^T_y\\ A^T_{xy} & D^T_{xy} & F^T_{xy}\end{bmatrix}\Delta T=-\sum_{k=1}^{N}\int_{h_{k-1}}^{h_k}\begin{bmatrix}A_x\\A_y\\A_{xy}\end{bmatrix}_k(1,Z,Z^3)\Delta T\,dZ\tag{27}$$

The boundary conditions expressed by Eq. (17) become
$x = 0, \pi$:

$$W = \Psi_y = 0, \ M_x = P_x = 0 \quad \text{(simply supported)} \tag{28a}$$

$$W = \Psi_x = \Psi_y = 0 \quad \text{(clamped)} \tag{28b}$$

and the immovable in-plane boundary condition of Eq. (19b) becomes

$$\begin{aligned}&\int_0^{2\pi}\int_0^{\pi}\left[\left(\gamma_{24}^2\beta^2\frac{\partial^2 F}{\partial y^2}-\gamma_5\frac{\partial^2 F}{\partial x^2}-\gamma_{213}\beta\frac{\partial^2 F}{\partial x\partial y}\right)+\gamma_{24}\left(\gamma_{511}\frac{\partial \Psi_x}{\partial x}+\gamma_{233}\beta\frac{\partial \Psi_y}{\partial y}\right)\right.\\&-\gamma_{24}\gamma_{223}\left(\beta\frac{\partial \Psi_x}{\partial y}+\frac{\partial \Psi_y}{\partial x}\right)-\varepsilon\gamma_{24}\left(\gamma_{611}\frac{\partial^2 W}{\partial x^2}\gamma_{244}\beta^2\frac{\partial^2 W}{\partial y^2}+2\gamma_{516}\beta\frac{\partial^2 W}{\partial x\partial y}\right)\\&\left.-\frac{1}{2}\gamma_{24}\left(\frac{\partial W}{\partial x}\right)^2+\varepsilon(\gamma_{24}^2\gamma_{T1}-\gamma_5\gamma_{T2}+\gamma_{213}\gamma_{T3})\Delta T\right]dxdy=0\end{aligned} \tag{29}$$

and the periodicity (or closed) condition becomes

$$\begin{aligned}&\int_0^{2\pi}\left[\left(\frac{\partial^2 F}{\partial x^2}-\gamma_5\beta^2\frac{\partial^2 F}{\partial y^2}-\gamma_{211}\beta\frac{\partial^2 F}{\partial x\partial y}\right)+\gamma_{24}\left(\gamma_{220}\frac{\partial \Psi_x}{\partial x}+\gamma_{522}\beta\frac{\partial \Psi_y}{\partial y}\right)\right.\\&+\gamma_{24}\gamma_{230}\left(\beta\frac{\partial \Psi_x}{\partial y}+\frac{\partial \Psi_y}{\partial x}\right)-\varepsilon\gamma_{24}\left(\gamma_{240}\frac{\partial^2 W}{\partial x^2}+\gamma_{622}\beta^2\frac{\partial^2 W}{\partial y^2}+2\gamma_{526}\beta\frac{\partial^2 W}{\partial x\partial y}\right)\\&\left.-\gamma_{24}W-\frac{1}{2}\gamma_{24}\beta^2\left(\frac{\partial W}{\partial y}\right)^2+\varepsilon(\gamma_{T2}-\gamma_5\gamma_{T1}+\gamma_{211}\gamma_{T3})\Delta T\right]dy=0\end{aligned} \tag{30}$$

In Eq. (26), we introduce an important parameter ε. As has been shown [6], in practice, the shell structure will have $\bar{Z} \geq 10$, so that we always have $\varepsilon << 1$. When $\varepsilon < 1$, Eqs. (21)–(24) are of the boundary layer type. Eqs. (21)–(24) need to be mathematically separated into two sets and solved in sequence. The first set of equations yields the particular solution of static deflection due to thermal bending stresses, and the second set of equations gives the homogeneous solution of vibration characteristics on the initial deflected shell. We apply a singular perturbation technique that involves a two-step perturbation process [36] to solve this nonlinear vibration problem of CNTRC laminated cylindrical shells. To this end, we assume that

$$\begin{aligned}W &= w(x, y, \tau, \varepsilon) + \tilde{W}(x, \xi, y, \tau, \varepsilon) + \hat{W}(x, \zeta, y, \tau, \varepsilon),\\ F &= f(x, y, \tau, \varepsilon) + \tilde{F}(x, \xi, y, \tau, \varepsilon) + \hat{F}(x, \zeta, y, \tau, \varepsilon),\\ \Psi_x &= \psi_x(x, y, \tau, \varepsilon) + \tilde{\Psi}_x(x, \xi, y, \tau, \varepsilon) + \hat{\Psi}_x(x, \zeta, y, \tau, \varepsilon),\\ \Psi_y &= \psi_y(x, y, \tau, \varepsilon) + \tilde{\Psi}_y(x, \xi, y, \tau, \varepsilon) + \hat{\Psi}_y(x, \zeta, y, \tau, \varepsilon),\end{aligned} \tag{31}$$

where $\tau = \varepsilon t$ and ε is a small perturbation parameter (provided $\bar{Z} > 2.96$) as defined in Eq. (26) and $w(x, y, \tau, \varepsilon)$, $f(x, y, \tau, \varepsilon)$, $\psi_x(x, y, \tau, \varepsilon)$, $\psi_y(x, y, \tau, \varepsilon)$ are called regular solutions of the shell, $\tilde{W}(x, \xi, y, \tau, \varepsilon)$, $\tilde{F}(x, \xi, y, \tau, \varepsilon)$, $\tilde{\Psi}_x(x, \xi, y, \tau, \varepsilon)$, $\tilde{\Psi}_y(x, \xi, y, \tau, \varepsilon)$ and $\hat{W}(x, \zeta, y, \tau, \varepsilon)$, $\hat{F}(x, \zeta, y, \tau, \varepsilon)$, $\hat{\Psi}_x(x, \zeta, y, \tau, \varepsilon)$, $\hat{\Psi}_y(x, \zeta, y, \tau, \varepsilon)$ are the boundary layer solutions near the $x = 0$ and $x = \pi$ edges, respectively. Furthermore, the regular and boundary layer solutions can be expressed in the forms of perturbation expansions as follows

$$\begin{aligned}&w(x, y, \tau, \varepsilon) = \sum_{j=1}\varepsilon^{j/2}w_{j/2}(x, y, \tau),\ f(x, y, \tau, \varepsilon) = \sum_{j=0}\varepsilon^{j/2}f_{j/2}(x, y, \tau),\\&\psi_x(x, y, \tau, \varepsilon) = \sum_{j=1}\varepsilon^{j/2}(\psi_x)_{j/2}(x, y, \tau),\ \psi_y(x, y, \tau, \varepsilon) = \sum_{j=1}\varepsilon^{j/2}(\psi_y)_{j/2}(x, y, \tau),\\&\tilde{W}(x, \xi, y, \tau, \varepsilon) = \sum_{j=0}\varepsilon^{j/2+1}\tilde{W}_{j/2+1}(x, \xi, y, \tau),\ \tilde{F}(x, \xi, y, \tau, \varepsilon) = \sum_{j=0}\varepsilon^{j/2+2}\tilde{F}_{j/2+2}(x, \xi, y, \tau),\\&\tilde{\Psi}_x(x, \xi, y, \tau, \varepsilon) = \sum_{j=0}\varepsilon^{(j+3)/2}(\tilde{\Psi}_x)_{(j+3)/2}(x, \xi, y, \tau)\ ,\end{aligned} \tag{32a}$$

Please cite this article as: H.-S. Shen, C. Li and J.N. Reddy, Large amplitude vibration of FG-CNTRC laminated cylindrical shells with negative Poisson's ratio, Computer Methods in Applied Mechanics and Engineering (2019) 112727, https://doi.org/10.1016/j.cma.2019.112727.

$$\tilde{\Psi}_y(x,\xi,y,\tau,\varepsilon)=\sum_{j=0}\ \varepsilon^{j/2+2}(\tilde{\Psi}_y)_{j/2+2}(x,\xi,y,\tau)\ , \tag{32b}$$

$$\hat{W}(x,\zeta,y,\tau,\varepsilon)=\sum_{j=0}\varepsilon^{j/2+1}\hat{W}_{j/2+1}(x,\zeta,y,\tau),\ \hat{F}(x,\zeta,y,\tau,\varepsilon)=\sum_{j=0}\varepsilon^{j/2+2}\hat{F}_{j/2+2}(x,\zeta,y,\tau),$$

$$\hat{\Psi}_x(x,\zeta,y,\tau,\varepsilon)=\sum_{j=0}\varepsilon^{(j+3)/2}(\hat{\Psi}_x)_{(j+3)/2}(x,\zeta,y,\tau),$$

$$\hat{\Psi}_y(x,\zeta,y,\tau,\varepsilon)=\sum_{j=0}\varepsilon^{j/2+2}(\hat{\Psi}_y)_{j/2+2}(x,\zeta,y,\tau), \tag{32c}$$

in which ξ and ζ are the boundary layer variables defined by

$$\xi=x/\sqrt{\varepsilon},\zeta=(\pi-x)/\sqrt{\varepsilon} \tag{33}$$

For the flexural vibration of the anisotropic laminated cylindrical shell, the initial transverse vibration mode of the shell in the space domain may be expressed as

$$w_2(x,y,\tau)=A_{00}^{(2)}+A_{11}^{(2)}(\tau)\sin mx\sin ny+a_{11}^{(2)}(\tau)\cos mx\cos ny \tag{34}$$

where $(m,\ n)$ are the half-waves of vibration mode of the shell along the axial and circumferential directions, respectively. The following initial conditions are considered in this study

$$W|_{\tau=0}=\frac{\partial W}{\partial\tau}|_{\tau=0}=0,\qquad \Psi_x|_{\tau=0}=\frac{\partial\Psi_x}{\partial\tau}|_{\tau=0}=0,\qquad \Psi_y|_{\tau=0}=\frac{\partial\Psi_y}{\partial\tau}|_{\tau=0}=0 \tag{35}$$

We can obtain a set of perturbation equations by substituting Eq. (31) into Eqs. (21)–(24) and collecting the terms of the same order of ε and then solve the perturbation equations step by step for the asymptotic solutions. Then by matching the regular solutions with the boundary layer solutions at the each end of the shell, one obtains

$$\begin{aligned}W(x,y,t)=\varepsilon^{3/2}&\left[A_{00}^{(3/2)}(t)-A_{00}^{(3/2)}(t)\left(a_{01}^{(3/2)}\cos\phi\frac{x}{\sqrt{\varepsilon}}+a_{10}^{(3/2)}\sin\phi\frac{x}{\sqrt{\varepsilon}}\right)\exp\left(-\vartheta\frac{x}{\sqrt{\varepsilon}}\right)\right.\\&\left.-A_{00}^{(3/2)}(t)\left(a_{01}^{(3/2)}\cos\phi\frac{\pi-x}{\sqrt{\varepsilon}}+a_{10}^{(3/2)}\sin\phi\frac{\pi-x}{\sqrt{\varepsilon}}\right)\exp\left(-\vartheta\frac{\pi-x}{\sqrt{\varepsilon}}\right)\right]\\&+\varepsilon^2[A_{11}^{(2)}(t)\sin mx\sin ny+a_{11}^{(2)}(t)\cos mx\cos ny\\&-(a_{11}^{(2)}(t)\cos ny)\left(a_{01}^{(1)}\cos\phi\frac{x}{\sqrt{\varepsilon}}+a_{10}^{(1)}\sin\phi\frac{x}{\sqrt{\varepsilon}}\right)\exp\left(-\vartheta\frac{x}{\sqrt{\varepsilon}}\right)\\&-(a_{11}^{(2)}(t)\cos ny)\left(a_{01}^{(1)}\cos\phi\frac{\pi-x}{\sqrt{\varepsilon}}+a_{10}^{(1)}\sin\phi\frac{\pi-x}{\sqrt{\varepsilon}}\right)\exp\left(-\vartheta\frac{\pi-x}{\sqrt{\varepsilon}}\right)\Big]\\&+\varepsilon^6\Big[A_{13}^{(6)}(t)\sin mx\sin 3ny+a_{13}^{(6)}(t)\cos mx\cos 3ny\\&+A_{31}^{(6)}(t)\sin 3mx\sin ny+a_{31}^{(6)}(t)\cos 3mx\cos ny\Big]+O(\varepsilon^7)\end{aligned} \tag{36}$$

$$\begin{aligned}\Psi_x(x,y,t)=\varepsilon^2&\left\{[C_{11}^{(2)}(t)+\ddot{C}_{11}^{(4)}(t)]\cos mx\sin ny+[c_{11}^{(2)}(t)+\ddot{c}_{11}^{(4)}(t)]\sin mx\cos ny\right.\\&+\left[A_{00}^{(3/2)}(t)\left(c_{01}^{(2)}\cos\phi\frac{x}{\sqrt{\varepsilon}}+c_{10}^{(2)}\sin\phi\frac{x}{\sqrt{\varepsilon}}\right)\exp\left(-\vartheta\frac{x}{\sqrt{\varepsilon}}\right)\right.\\&\left.\left.+A_{00}^{(3/2)}(t)\left(c_{01}^{(2)}\cos\phi\frac{\pi-x}{\sqrt{\varepsilon}}+c_{10}^{(2)}\sin\phi\frac{\pi-x}{\sqrt{\varepsilon}}\right)\exp\left(-\vartheta\frac{\pi-x}{\sqrt{\varepsilon}}\right)\right]\right\}\\&+\varepsilon^3\{[C_{11}^{(3)}(t)+\ddot{C}_{11}^{(5)}(t)]\cos mx\sin ny+[c_{11}^{(3)}(t)+\ddot{c}_{11}^{(5)}(t)]\sin mx\cos ny\}\\&+\varepsilon^4\{[C_{20}^{(4)}(t)+\ddot{C}_{20}^{(6)}(t)]\sin 2mx+[c_{02}^{(4)}(t)+\ddot{c}_{02}^{(6)}(t)]\sin 2ny\}\\&+\varepsilon^6\Big[C_{13}^{(6)}(t)\cos mx\sin 3ny+c_{13}^{(6)}(t)\sin mx\cos 3ny\\&+C_{31}^{(6)}(t)\cos 3mx\sin ny+c_{31}^{(6)}(t)\sin 3mx\cos ny\Big]+O(\varepsilon^7)\end{aligned} \tag{37}$$

Please cite this article as: H.-S. Shen, C. Li and J.N. Reddy, Large amplitude vibration of FG-CNTRC laminated cylindrical shells with negative Poisson's ratio, Computer Methods in Applied Mechanics and Engineering (2019) 112727, https://doi.org/10.1016/j.cma.2019.112727.

$$\begin{aligned}\Psi_y(x,y,t) &= \varepsilon^2\{[D_{11}^{(2)}(t)+\ddot{D}_{11}^{(4)}(t)]\sin mx\cos ny+[d_{11}^{(2)}(t)+\ddot{d}_{11}^{(4)}(t)]\cos mx\sin ny\\ &+\left[A_{00}^{(3/2)}(t)\left(d_{01}^{(2)}\cos\phi\frac{x}{\sqrt{\varepsilon}}+d_{10}^{(2)}\sin\phi\frac{x}{\sqrt{\varepsilon}}\right)\exp\left(-\vartheta\frac{x}{\sqrt{\varepsilon}}\right)\right.\\ &\left.+A_{00}^{(3/2)}(t)\left(d_{01}^{(2)}\cos\phi\frac{\pi-x}{\sqrt{\varepsilon}}+d_{10}^{(2)}\sin\phi\frac{\pi-x}{\sqrt{\varepsilon}}\right)\exp\left(-\vartheta\frac{\pi-x}{\sqrt{\varepsilon}}\right)\right]\Big\}\\ &+\varepsilon^3\{[D_{11}^{(3)}(t)+\ddot{D}_{11}^{(5)}(t)]\sin mx\cos ny+[d_{11}^{(3)}(t)+\ddot{d}_{11}^{(5)}(t)]\cos mx\sin ny\}\\ &+\varepsilon^4\{[D_{02}^{(4)}(t)+\ddot{D}_{02}^{(6)}(t)]\sin 2ny+[d_{20}^{(4)}(t)+\ddot{d}_{20}^{(6)}(t)]\sin 2mx\}\\ &+\varepsilon^6\Big[D_{13}^{(6)}(t)\sin mx\cos 3ny+d_{13}^{(6)}(t)\cos mx\sin 3ny\\ &+D_{31}^{(6)}(t)\sin 3mx\cos ny+d_{31}^{(6)}(t)\cos 3mx\sin ny\Big]+O(\varepsilon^7)\end{aligned}\tag{38}$$

$$\begin{aligned}F(x,y,t) &= -B_{00}^{(0)}\frac{y^2}{2}-b_{00}^{(0)}\frac{x^2}{2}-C_{00}^{(0)}xy\\ &+\varepsilon^2\{[B_{11}^{(2)}(t)+\ddot{B}_{11}^{(4)}(t)]\sin mx\sin ny+\ddot{b}_{11}^{(4)}(t)\cos mx\cos ny\}\\ &+\varepsilon^{5/2}\left[A_{00}^{(3/2)}(t)\left(b_{01}^{(5/2)}\cos\phi\frac{x}{\sqrt{\varepsilon}}+b_{10}^{(5/2)}\sin\phi\frac{x}{\sqrt{\varepsilon}}\right)\exp\left(-\vartheta\frac{x}{\sqrt{\varepsilon}}\right)\right.\\ &\left.+A_{00}^{(3/2)}(t)\left(b_{01}^{(5/2)}\cos\phi\frac{\pi-x}{\sqrt{\varepsilon}}+b_{10}^{(5/2)}\sin\phi\frac{\pi-x}{\sqrt{\varepsilon}}\right)\exp\left(-\vartheta\frac{\pi-x}{\sqrt{\varepsilon}}\right)\right]\\ &+\varepsilon^3\{[B_{11}^{(3)}(t)+\ddot{B}_{11}^{(5)}(t)]\sin mx\sin ny+[b_{11}^{(3)}(t)+\ddot{b}_{11}^{(5)}(t)]\cos mx\cos ny\}\\ &+\varepsilon^4\left\{\left[-B_{00}^{(4)}\frac{y^2}{2}-b_{00}^{(4)}\frac{x^2}{2}-C_{00}^{(4)}xy\right]\right.\\ &\left.+[B_{20}^{(4)}(t)+\ddot{B}_{20}^{(6)}(t)]\cos 2mx+[B_{02}^{(4)}(t)+\ddot{B}_{02}^{(6)}(t)]\cos 2ny\right\}\\ &+\varepsilon^6\Big[B_{13}^{(6)}(t)\sin mx\sin 3ny+b_{13}^{(6)}(t)\cos mx\cos 3ny\\ &+B_{31}^{(6)}(t)\sin 3mx\sin ny+b_{31}^{(6)}(t)\cos 3mx\cos ny\Big]+O(\varepsilon^7)\end{aligned}\tag{39}$$

and the non-dimensional transverse load yields

$$\begin{aligned}\lambda_q(x,y,t) &= [(\varepsilon^2A_{11}^{(2)}(t))g_{11}^{(2)}+(\varepsilon^2\ddot{A}_{11}^{(2)}(t))g_{11}^{(4)}]\sin mx\sin ny+[(\varepsilon^2\ddot{A}_{11}^{(2)}(t))q_{11}^{(4)}]\cos mx\cos ny\\ &+\varepsilon[(\varepsilon^2A_{11}^{(2)}(t))g_{11}^{(3)}+(\varepsilon^2\ddot{A}_{11}^{(2)}(t))g_{11}^{(5)}]\sin mx\sin ny\\ &+\varepsilon^2[(\varepsilon^2A_{11}^{(2)}(t))g_{11}^{(4)}+(\varepsilon^2\ddot{A}_{11}^{(2)}(t))g_{11}^{(6)}]\sin mx\sin ny\\ &+\varepsilon^2[(\varepsilon^2\ddot{A}_{11}^{(1)}(t))q_{11}^{(6)}]\cos mx\cos ny+[(\varepsilon^2A_{11}^{(2)}(t))^2g_{20}^{(4)}+(\varepsilon^2\ddot{A}_{11}^{(2)}(t))^2g_{20}^{(6)}]\cos 2mx\\ &+(\varepsilon^2A_{11}^{(2)}(t))^2g_{02}^{(4)}\cos 2ny+(\varepsilon^2A_{11}^{(2)}(t))^3[g_{11}^{(6)}\sin mx\sin ny]\\ &+(\varepsilon^2A_{11}^{(2)}(t))^5[g_{11}^{(10)}\sin mx\sin ny+q_{11}^{(10)}\cos mx\cos ny]+O(\varepsilon^{11})\end{aligned}\tag{40}$$

Note that in Eqs. (36)–(40) τ is replaced back by t. Note that the solutions of Eqs. (36)–(40) are different from those obtained in Shen and Xiang [25]. For the case of free vibration, one has $\lambda_q = 0$. Then, the Duffing-type equation is obtained by applying Galerkin procedure to Eq. (40)

$$G_{30}\frac{d^2(A_{11}^{(2)}\varepsilon^2)}{dt^2}+G_{31}(A_{11}^{(2)}\varepsilon^2)+G_{32}(A_{11}^{(2)}\varepsilon^2)^2+G_{33}(A_{11}^{(2)}\varepsilon^2)^3+G_{35}(A_{11}^{(2)}\varepsilon^2)^5=0\tag{41}$$

In the second step, $(A_{11}^{(2)}\varepsilon^2)$ is taken as the second perturbation parameter relating to the dimensionless maximum deflection W_{max}. Accordingly, the solution of Eq. (41) is obtained as

$$\omega_{NL}=\omega_L\left[1+G_2A^2+G_4A^4+\cdots\right]\tag{42}$$

When $\Delta T = 0$, we have $G_{32} = 0$, in such a case the solution of Eq. (41) may be simply written as

$$\omega_{NL}=\omega_L\left[1+\frac{3}{4}\frac{G_{33}}{G_{31}}A^2+\frac{5}{8}\frac{G_{35}}{G_{31}}A^4\right]^{1/2}\tag{43}$$

Please cite this article as: H.-S. Shen, C. Li and J.N. Reddy, Large amplitude vibration of FG-CNTRC laminated cylindrical shells with negative Poisson's ratio, Computer Methods in Applied Mechanics and Engineering (2019) 112727, https://doi.org/10.1016/j.cma.2019.112727.

Table 1
Temperature-dependent material properties for (10, 10) SWCNT (tube length = 9.26 nm, tube mean radius = 0.68 nm, tube thickness = 0.067 nm, $\nu_{12}^{CN} = 0.175$) [37].

Temperature (K)	E_{11}^{CN}(TPa)	E_{22}^{CN}(TPa)	G_{12}^{CN}(TPa)	$\alpha_{11}^{CN}(\times 10^{-6}/\mathrm{K})$	$\alpha_{22}^{CN}(\times 10^{-6}/\mathrm{K})$
300	5.6466	7.0800	1.9445	3.4584	5.1682
400	5.5679	6.9814	1.9703	4.1496	5.0905
500	5.5308	6.9348	1.9643	4.5361	5.0189

Table 2
Efficiency parameters for CNT/PmPV nanocomposites [24].

V_{CN}	η_1	η_2	η_3
0.11	0.149	0.934	0.934
0.14	0.150	0.941	0.941
0.17	0.149	1.381	1.381

Table 3
Negative Poisson's ratios ν_{13} for $(\pm 22)_{3T}$ and ν_{23} for $(\pm 70)_{3T}$ CNTRC laminated cylindrical shells at $\bar{W}/h = 0$ ($h = 3$ mm).

T(K)	UD	FG-V	FG-Λ	FG-X	FG-O
$(\pm 22)_{3T}$					
300	−0.63	−0.56	−0.56	−0.54	−0.57
400	−0.74	−0.67	−0.67	−0.65	−0.68
500	−0.90	−0.83	−0.83	−0.81	−0.84
$(\pm 70)_{3T}$					
300	−0.63	−0.55	−0.55	−0.53	−0.56
400	−0.77	−0.69	−0.69	−0.66	−0.70
500	−0.97	−0.88	−0.88	−0.86	−0.90

where $A = W_{max}$ is the dimensionless amplitude of the shell and the corresponding linear frequency as defined in Eq. (26) is given by $\Omega_L = \omega_L(\pi/L)(E_0/\rho_0)^{1/2}$, where $\omega_L = [G_{31}/G_{30}]^{1/2}$. All symbols used in Eqs. (41) and (42) may be found in Appendix C.

4. Numerical results and discussion

Numerical results are presented in this section for the nonlinear vibration of CNTRC laminated cylindrical shells in thermal environmental conditions. In the current study, it is assumed that properties of the constituents of CNTRC layers are temperature dependent. (10, 10) SWCNTs with $h_{CN} = 0.067$ nm and $\rho^{CN} = 1400$ kg/m^3 are selected as reinforcements. Temperature-dependent material properties of (10, 10) SWCNTs are listed in Table 1 [37]. The CNT efficiency parameters η_j ($j = 1, 2, 3$) are obtained by matching the Young's moduli E_{11} and E_{22} of CNTRCs predicted from the Voigt model to those from the MD simulations, as previously reported in Shen [24]. These parameters are listed in Table 2, and we also assume that $\eta_3 = \eta_2$ and $G_{23} = G_{13} = G_{12}$. Poly{(m-phenylenevinylene)-co-[(2,5-dioctoxy-p-phenylene) vinylene]}, referred to as PmPV, is selected for the matrix, and the material properties of PmPV are assumed to be $\rho^m = 1150$ kg/m^3, $\nu^m = 0.34$, $\alpha^m = 45(1+0.0005\Delta T)\times 10^{-6}$/K and $E^m = (3.51 - 0.0047T)$ GPa, in which $T = T_0 + \Delta T$ and $T_0 = 300$ K (room temperature). Hence, we have $\alpha^m = 45.0 \times 10^{-6}$/K and $E^m = 2.1$ GPa when $T = 300$ K. From Eqs. (4) and (5), Figs. 1 and 2 present the relationships between the effective Poisson's ratios (EPRs) and the lamination angles. The results show that the maximum negative Poisson's ratio ν_{13} is at a lamination angle of around 22°, while the maximum negative Poisson's ratio ν_{23} is at a lamination angle of around 70°. Hence, $(\pm 22)_{3T}$ and $(\pm 70)_{3T}$ CNTRC laminated cylindrical shells are considered in the following examples. The negative Poisson's ratios ν_{13} and ν_{23} for $(\pm 22)_{3T}$ and $(\pm 70)_{3T}$ CNTRC laminated cylindrical shells under different thermal environmental conditions $T = 300$, 400 and 500 K are listed in Table 3.

Please cite this article as: H.-S. Shen, C. Li and J.N. Reddy, Large amplitude vibration of FG-CNTRC laminated cylindrical shells with negative Poisson's ratio, Computer Methods in Applied Mechanics and Engineering (2019) 112727, https://doi.org/10.1016/j.cma.2019.112727.

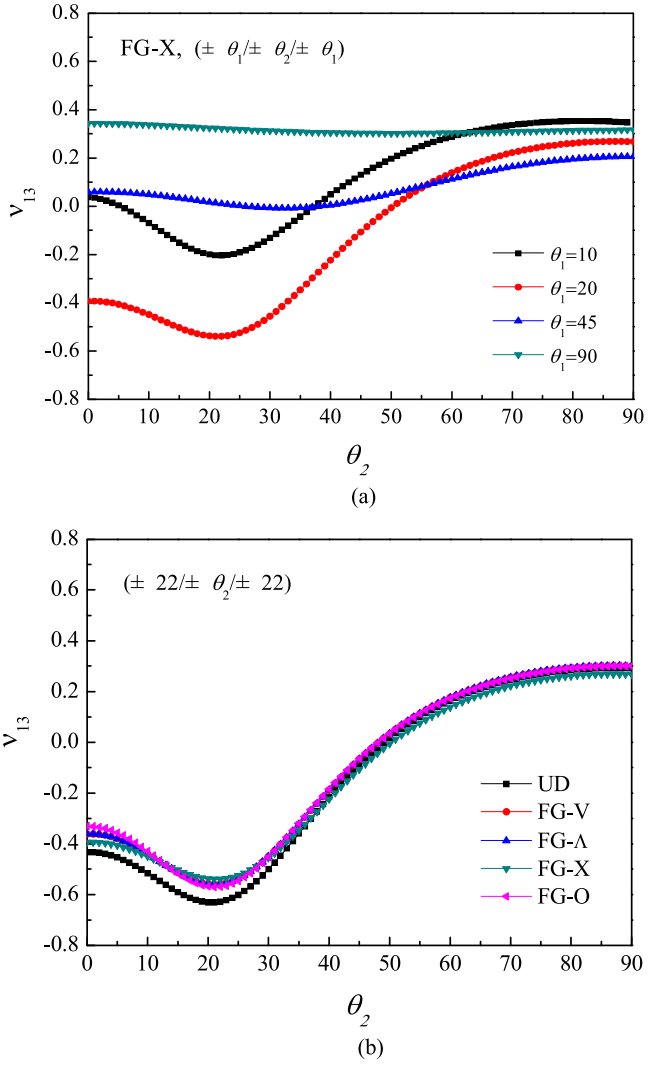

Fig. 1. Poisson's ratio ν_{13} for $(\pm\theta_1/\pm\theta_2/\pm\theta_1)$ laminates.

As part of the validation of the present solution method, the linear dimensionless frequencies $\tilde{\omega} = \Omega(L^2/100h)\sqrt{\rho/E_{22}}$ for angle-ply laminated cylindrical shells with four types of configurations are calculated and compared in Table 4 with the DQM results of Malekzadeh et al. [38] based on the first-order shear deformation shell theory. The computing data adopted are: $E_{11}/E_{22} = 40$, G_{12}/E_{22}=$G_{13}/E_{22} = 0.6$, $G_{23}/E_{22} = 0.5$, $\nu_{12} = 0.25$, $\rho = 1$, $L/R = 1$, $R/h = 10$. It can be seen that the present theoretical and FEM results are lower than those of Malekzadeh et al. [38]. As a second example, the linear dimensionless frequencies $\tilde{\Omega} = \Omega(R^2/h)\sqrt{\rho_0/E_0}$ for UD and FG CNTRC cylindrical shells with $R/h = 10$, $h = 5$ mm and $\bar{Z} = 100$ and 500 at $T = 300$ K are calculated and compared in Table 5 with the DQM results of Ansari et al. [39] based on the first-order shear deformation shell theory with shear factor is taken to be 5/6. In Table 5, the extended rule of mixture is adopted and the CNT efficiency parameters are taken to be $\eta_1 = 0.137$, $\eta_2 = 1.022$ and $\eta_3 = 0.715$ for the case of $V^*_{CN} = 0.12$, and $\eta_1 = 0.142$, $\eta_2 = 1.626$ and $\eta_3 = 1.138$ for the case of $V^*_{CN} = 0.17$, and $\eta_1 = 0.141$, $\eta_2 = 1.585$ and $\eta_3 = 1.109$ for the case of $V^*_{CN} = 0.28$. It is observed that the present theoretical and FEM results agree reasonably well with each other, whereas the DQM results of Ansari et al. [39] are higher than present theoretical solutions for the FG-Λ shells, but lower than present theoretical solutions for the FG-X shells. As a third example, the nonlinear-to-linear frequency ratios ω_{NL}/ω_L for an orthotropic cylindrical shell are plotted in Fig. 3 and are compared with the Galerkin method

Please cite this article as: H.-S. Shen, C. Li and J.N. Reddy, Large amplitude vibration of FG-CNTRC laminated cylindrical shells with negative Poisson's ratio, Computer Methods in Applied Mechanics and Engineering (2019) 112727, https://doi.org/10.1016/j.cma.2019.112727.

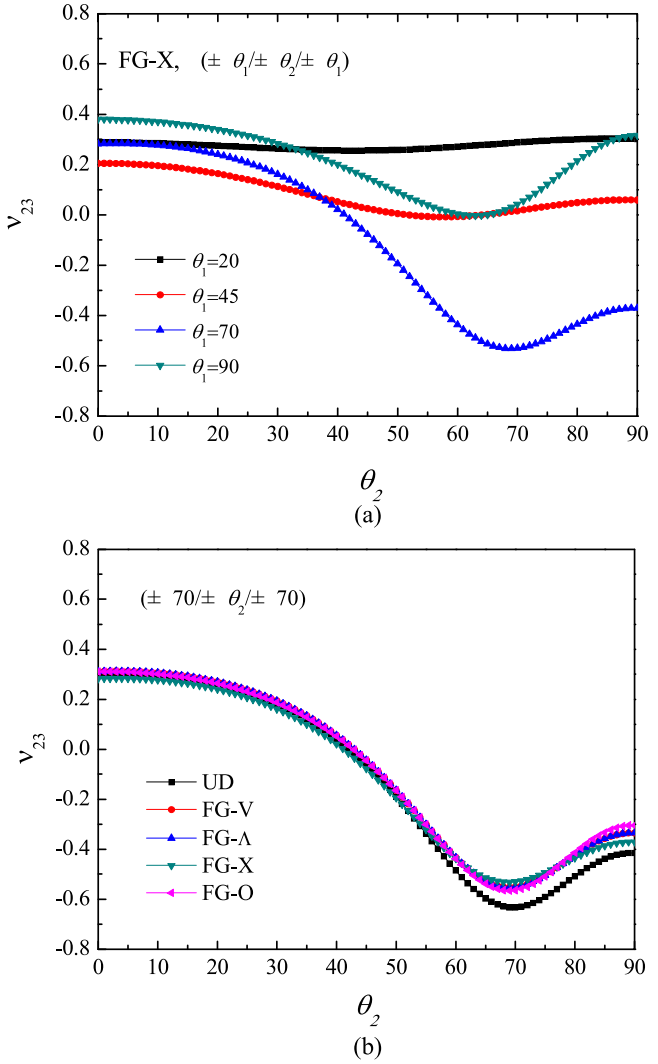

Fig. 2. Poisson's ratio ν_{23} for $(\pm\theta_1/\pm\theta_2/\pm\theta_1)$ laminates.

results of Nowinski [40], the FEM results of Lakis et al. [1]. The computing data adopted are: $L = 0.4$ m, $R = 0.254$ m, $h = 2.54$ mm, $E_{11} = 200$ GPa, $E_{22} = G_{12} = 0.05E_{11}$, $\nu_{12} = 0.2$, $\rho = 7800$ kg/m^3 and the vibration mode is taken to be $(m, n) = (1, 4)$. It is observed that the present FEM results lie between the present theoretical solution and the Galerkin method solution of Nowinski [40]. The FEM results of Lakis et al. [1] are much higher than others. As pointed out in Shen [36], the nonlinearity of the present solution is much weaker than that of Lakis et al. [1] and stronger than that of Nowinski [40]. The difference between the results obtained by the present theory and those of [1,40] might be due to the different shell theories and the different expansions of modal shape functions.

A parametric study has been carried out and typical results are shown in Tables 6 and 7 and Figs. 4–8. For these examples, the shell geometric parameters $\bar{Z} = (L^2/Rh) = 100$, 300, 500, 600 and 800, $R/h = 30$, the thickness of each ply is identical and the total thickness of the shell $h = 3$ mm. The dimensionless natural frequency is defined by $\tilde{\Omega} = \Omega(R^2/h)\sqrt{\rho_0/E_0}$, where ρ_0 and E_0 are the reference values of ρ^m and E^m at $\Delta T = 300$ K. Four types of FG-CNTRC shells, i.e. FG-Λ, FG-V, FG-O and FG-X, are considered. An UD-FRC shell with the same thickness is also considered as a comparator. The end condition is assumed to be simply supported and the in-plane condition is assumed to be immovable except for the cases in Table 7 and Fig. 6. A finite element commercial software has been

Please cite this article as: H.-S. Shen, C. Li and J.N. Reddy, Large amplitude vibration of FG-CNTRC laminated cylindrical shells with negative Poisson's ratio, Computer Methods in Applied Mechanics and Engineering (2019) 112727, https://doi.org/10.1016/j.cma.2019.112727.

Table 4
Comparison of dimensionless frequencies $\Omega(L^2/100h)\sqrt{\rho/E_{22}}$ for angle-ply laminated cylindrical shells.

		(m, n)[a]			
Lay-up	Source	(1, 1)	(1, 2)	(2, 1)	(2, 2)
$(15/-15)_{2T}$	Present (theoretical)	0.1640	0.1694	0.3741	0.3803
	Present (FEM)	0.1482	0.1665	0.3598	0.3663
	Malekzadeh et al. [38]	0.1950	0.2011	0.4466	0.4538
$(30/-30)_{2T}$	Present (theoretical)	0.1629	0.1852	0.3485	0.3643
	Present (FEM)	0.1596	0.1789	0.3356	0.3475
	Malekzadeh et al. [38]	0.1912	0.2192	0.4172	0.4364
$(45/-45)_{2T}$	Present (theoretical)	0.1886	0.2445	0.3141	0.3419
	Present (FEM)	0.1801	0.2289	0.3024	0.3249
	Malekzadeh et al. [38]	0.2097	0.2731	0.3695	0.4031
$(60/-60)_{2T}$	Present (theoretical)	0.3307	0.3331	0.3479	0.3964
	Present (FEM)	0.2629	0.2722	0.3335	0.3751
	Malekzadeh et al. [38]	0.3063	0.3017	0.3853	0.4432

[a]Vibration mode

Table 5
Comparison of dimensionless frequencies $\tilde{\Omega} = \Omega(R^2/h)\sqrt{\rho_0/E_0}$ for CNT/PMMA cylindrical shells [$R/h = 10$, $h = 5$ mm, $T = 300$ K, $(m, n) = (1, 2)$].

		$\bar{Z} = 100$			$\bar{Z} = 500$		
V^*_{CN}	Source	UD	FG-Λ	FG-X	UD	FG-Λ	FG-X
0.12	Ansari et al. [39]	3.3656	3.2019	3.5674	1.7020	1.6614	1.6977
	Present (theoretical)	3.3704	3.1568	3.6150	1.7231	1.6652	1.7814
	Present (FEM)	3.4142	3.2173	3.5634	1.6746	1.5976	1.7361
0.17	Ansari et al. [39]	4.2870	4.1155	4.5410	2.1900	2.1486	2.1913
	Present (theoretical)	4.2866	4.0412	4.6106	2.2106	2.1477	2.3121
	Present (FEM)	4.3475	4.1206	4.5435	2.1357	2.0498	2.2272
0.28	Ansari et al. [39]	4.6543	4.5410	5.2014	2.3178	2.3228	2.3675
	Present (theoretical)	4.6766	4.4886	5.2173	2.3548	2.3306	2.5651
	Present (FEM)	4.7266	4.5648	5.0169	2.3096	2.2602	2.4674

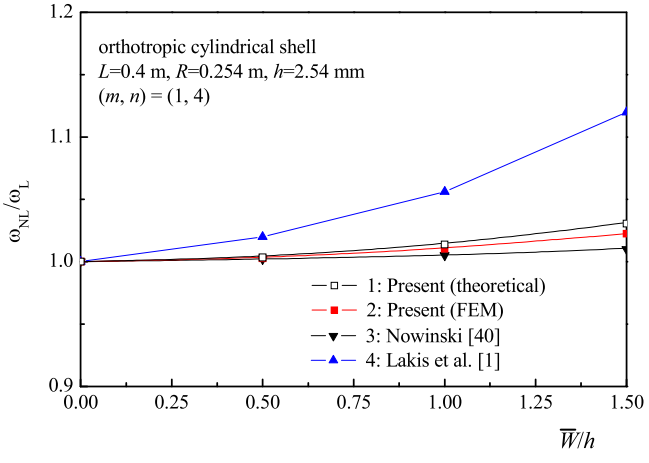

Fig. 3. Comparisons of frequency–amplitude curves for an orthotropic cylindrical shell.

Please cite this article as: H.-S. Shen, C. Li and J.N. Reddy, Large amplitude vibration of FG-CNTRC laminated cylindrical shells with negative Poisson's ratio, Computer Methods in Applied Mechanics and Engineering (2019) 112727, https://doi.org/10.1016/j.cma.2019.112727.

Table 6
Natural frequency $\tilde{\Omega} = \Omega(R^2/h)\sqrt{\rho_0/E_0}$ of CNTRC laminated cylindrical shells ($R/h = 30$, $h = 3$ mm, $T = 300$ K)

Lay-up	$\bar{Z}$		(m, n)[a]				
			(1, 1)	(1, 2)	(1, 3)	(1, 4)	(1, 5)
$(\pm 22)_{3T}$	600	UD	32.9389	17.8734	9.4046	9.2710	12.2177
		FG-V	34.2380	17.9035	9.5349	9.4545	12.5351
		FG-Λ	34.2297	17.9164	9.5875	9.5148	12.5824
		FG-X	34.2382	17.9467	9.7652	9.9778	13.3362
		FG-O	34.2311	17.8835	9.3981	9.0555	11.8507
	800	UD	32.1659	13.6201	7.5794	8.4624	11.6965
		FG-V	32.9953	13.7110	7.7078	8.6564	12.0327
		FG-Λ	32.9888	13.7308	7.7609	8.7075	12.0704
		FG-X	32.9953	13.7601	7.9557	9.1766	12.8172
		FG-O	2.9900	13.6919	7.5510	8.2394	11.3409
$(\pm 70)_{3T}$	600	UD	15.3435	8.3712	16.0528	27.1558	40.4928
		FG-V	16.3906	8.4159	15.9003	26.9717	40.3803
		FG-Λ	16.3845	8.4123	15.8992	26.9713	40.3801
		FG-X	16.4064	8.8255	16.8041	28.3485	42.1602
		FG-O	16.3758	8.1557	15.3479	26.1830	39.4652
	800	UD	11.5327	7.9128	15.9288	27.0656	40.4119
		FG-V	12.3303	7.9004	15.7695	26.8797	40.2981
		FG-Λ	12.3256	7.8980	15.7688	26.8794	40.2979
		FG-X	12.3513	8.3256	16.6706	28.2525	42.0746
		FG-O	12.3134	7.6308	15.2195	26.0937	39.3852
$(\pm 45)_{3T}$	600	UD	30.4945	7.5226	10.8983	17.7691	26.5167
		FG-V	32.0258	7.7266	10.8265	17.6409	26.3720
		FG-Λ	32.0289	7.7464	10.8409	17.6496	26.3776
		FG-X	32.0365	7.9832	11.4746	18.6859	27.8560
		FG-O	32.0217	7.5782	10.4121	16.9657	25.4244
	800	UD	20.0265	6.4032	10.4933	17.4412	26.2132
		FG-V	21.2264	6.5119	10.4126	17.3141	26.0693
		FG-Λ	21.2308	6.5299	10.4239	17.3207	26.0736
		FG-X	21.2397	6.7831	11.0486	18.3456	27.5430
		FG-O	21.2217	6.3506	10.0013	16.6434	25.1239

[a]Vibration mode

used in order to perform the EPR-deflection curves. It should be appreciated that in Figs. 4–8 $\bar{W}/h$ and ω_{NL}/ω_L denote the dimensionless maximum deflection and the nonlinear-to-linear frequency ratio of the shell, respectively.

Table 6 presents the natural frequencies of $(\pm 22)_{3T}$, $(\pm 70)_{3T}$ and $(\pm 45)_{3T}$ CNTRC laminated cylindrical shells with $\bar{Z} = 600$ and 800 at T= 300K. In the current study, both Poisson's ratios ν_{13} and ν_{23} are positive for the $(\pm 45)_{3T}$ shell. The results for FG-Λ, FG-V, FG-O and FG-X shells are listed and the same shell of UD type are also listed for direct comparison. Note that only UD $(\pm 22)_{3T}$, $(\pm 70)_{3T}$ and $(\pm 45)_{3T}$ laminated shells are antisymmetric. It is observed that the $(\pm 22)_{3T}$ shell has fundamental frequencies and corresponding vibration mode $(m, n) = (1, 4)$ when $\bar{Z} = 600$, while it has fundamental frequencies and corresponding vibration mode $(m, n) = (1, 3)$ when $\bar{Z} = 800$. In contrast, both $(\pm 70)_{3T}$ and $(\pm 45)_{3T}$ shells have fundamental frequencies and corresponding vibration mode $(m, n) = (1, 2)$. It is found that the FG-X shell has the largest, while the FG-O shell has the lowest fundamental frequencies among the five shells. In contrast, for the $(\pm 45)_{3T}$ shell, the FG-X shell has the largest, while the UD shell has the lowest fundamental frequencies when $\bar{Z} = 600$.

Table 7 shows the effect of temperature variation on the fundamental frequency of $(\pm 22)_{3T}$, $(\pm 70)_{3T}$ and $(\pm 45)_{3T}$ CNTRC laminated cylindrical shells with movable and immovable end conditions. The thermal environments are taken to be $T = 300$, 400 and 500 K. As expected, the fundamental frequencies are the same for two different end conditions when $T = 300$ K. For the cases of $T = 400$ and 500 K, the fundamental frequencies of $(\pm 22)_{3T}$ shell with immovable end conditions are higher than those of the same shells with movable end conditions. In contrast,

Please cite this article as: H.-S. Shen, C. Li and J.N. Reddy, Large amplitude vibration of FG-CNTRC laminated cylindrical shells with negative Poisson's ratio, Computer Methods in Applied Mechanics and Engineering (2019) 112727, https://doi.org/10.1016/j.cma.2019.112727.

Table 7
Effect of temperature variations on the fundamental frequency of CNTRC laminated cylindrical shells ($R/h = 30$, $h = 3$ mm) with movable and immovable end conditions.

$\bar{Z}$	Lay-up	T(K)	UD	FG-V	FG-Λ	FG-X	FG-O
End condition: movable							
300	$(\pm22)_{3T}$	300	13.0579[a]	13.2118[a]	13.2834[a]	13.7182[a]	12.8710[a]
		400	12.5488[a]	12.6861[a]	12.7539[a]	13.1581[a]	12.3822[a]
		500	11.9377[a]	12.0658[a]	12.1283[a]	12.4987[a]	11.8027[a]
	$(\pm70)_{3T}$	300	10.8622[c]	11.1888[c]	11.1793[c]	11.5270[c]	10.9703[c]
		400	10.1865[c]	10.4497[c]	10.4416[c]	10.7907[c]	10.2324[c]
		500	9.4466[c]	9.6384[c]	9.6320[c]	9.9798[c]	9.4257[c]
	$(\pm45)_{3T}$	300	12.6935[b]	12.6955[b]	12.7194[b]	13.3730[b]	12.2779[b]
		400	12.2269[c]	12.2866[b]	12.3059[b]	12.9388[b]	11.8883[b]
		500	10.9137[c]	11.3827[c]	11.3973[c]	11.6020[c]	11.2604[c]
500	$(\pm22)_{3T}$	300	9.9669[a]	10.1441[a]	10.2095[a]	10.6668[a]	9.7589[a]
		400	9.4994[a]	9.6437[a]	9.7051[a]	10.1307[a]	9.2999[a]
		500	8.9662[a]	9.0776[a]	9.1331[a]	9.5245[a]	8.7789[a]
	$(\pm70)_{3T}$	300	8.7942[c]	8.8905[c]	8.8858[c]	9.2861[c]	8.6387[c]
		400	8.4352[c]	8.4992[c]	8.4953[c]	8.8893[c]	8.2535[c]
		500	7.8576[c]	8.0832[c]	8.0802[c]	8.4626[c]	7.6181[c]
	$(\pm45)_{3T}$	300	8.5241[c]	8.8106[c]	8.8313[c]	9.0554[c]	8.6716[c]
		400	7.9472[c]	8.1835[c]	8.2011[c]	8.4323[c]	8.0407[c]
		500	7.3131[c]	7.4892[c]	7.5030[c]	7.7431[c]	7.3420[c]
End condition: immovable							
300	$(\pm22)_{3T}$	300	13.0579[a]	13.2118[a]	13.2834[a]	13.7182[a]	12.8710[a]
		400	12.6902[a]	12.8325[a]	12.8996[a]	13.2993[a]	12.5323[a]
		500	12.1760[a]	12.3167[a]	12.3779[a]	12.7409[a]	12.0593[a]
	$(\pm70)_{3T}$	300	10.8622[c]	11.1888[c]	11.1793[c]	11.5270[c]	10.9703[c]
		400	10.0152[c]	10.2568[c]	10.2486[c]	10.6041[c]	10.0354[c]
		500	9.1698[c]	9.3247[c]	9.3182[c]	9.6772[c]	9.1048[c]
	$(\pm45)_{3T}$	300	12.6935[b]	12.6955[b]	12.7194[b]	13.3730[b]	12.2779[b]
		400	12.2030[c]	12.2584[b]	12.2778[b]	12.9121[b]	11.8592[b]
		500	10.8745[c]	11.3381[c]	11.3527[c]	11.5582[c]	11.2154[c]
500	$(\pm22)_{3T}$	300	9.9669[a]	10.1441[a]	10.2095[a]	10.6668[a]	9.7589[a]
		400	9.6140[a]	9.7619[a]	9.8226[a]	10.2433[a]	9.4225[a]
		500	9.1613[a]	9.2827[a]	9.3369[a]	9.7201[a]	8.9910[a]
	$(\pm70)_{3T}$	300	8.7942[c]	8.8905[c]	8.8858[c]	9.2861[c]	8.6387[c]
		400	8.3113[c]	8.3571[c]	8.3531[c]	8.7536[c]	8.1071[c]
		500	7.8576[c]	7.8595[c]	7.8565[c]	8.2492[c]	7.6181[c]
	$(\pm45)_{3T}$	300	8.5241[c]	8.8106[c]	8.8313[c]	9.0554[c]	8.6716[c]
		400	7.9254[c]	8.1584[c]	8.1760[c]	8.4079[c]	8.0152[c]
		500	7.2782[c]	7.4490[c]	7.4629[c]	7.7042[c]	7.3010[c]

[a]Vibration mode $(m, n) = (1, 4)$,
[b]$(m, n) = (1, 3)$,
[c]$(m, n) = (1, 2)$.

the fundamental frequencies of $(\pm70)_{3T}$ and $(\pm45)_{3T}$ shells with immovable end condition are lower than those of the same shell with movable end condition. The results confirm that the fundamental frequencies are decreased as temperature rises.

Fig. 4 presents the frequency–amplitude curves of $(\pm22)_{3T}$ and $(\pm70)_{3T}$ CNTRC laminated cylindrical shells with different types of CNT reinforcements at $T = 300$ K. The shell geometric parameter $\bar{Z} = 600$. The curves for FG-Λ, FG-V, FG-O and FG-X shells are plotted and compared with that of the same shell of UD type. The results show that for both $(\pm22)_{3T}$ and $(\pm70)_{3T}$ shells, the FG-X shells have the highest fundamental frequencies

Please cite this article as: H.-S. Shen, C. Li and J.N. Reddy, Large amplitude vibration of FG-CNTRC laminated cylindrical shells with negative Poisson's ratio, Computer Methods in Applied Mechanics and Engineering (2019) 112727, https://doi.org/10.1016/j.cma.2019.112727.

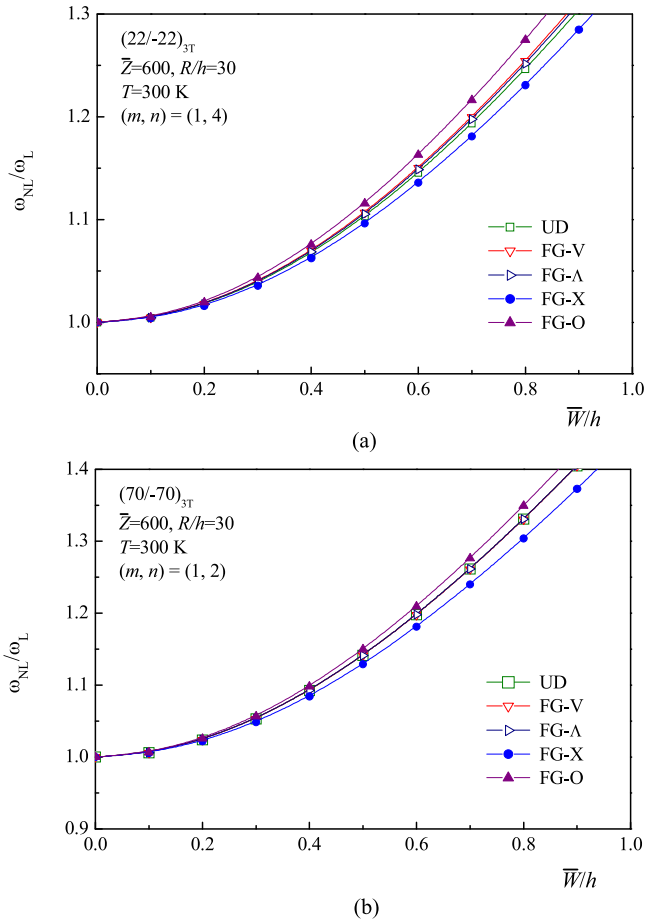

Fig. 4. Nonlinear vibration behaviors of CNTRC laminated cylindrical shells with negative Poisson's ratios: (a) $(\pm 22)_{3T}$ shells; (b) $(\pm 70)_{3T}$ shells.

(see Table 6), but the lowest nonlinear-to-linear frequency ratios among the five cases, while the FG-O shells have the lowest fundamental frequencies (see Table 6), but the highest nonlinear-to-linear frequency ratios among the same five cases. In contrast, the nonlinear-to-linear frequency ratio curves of UD, FG-Λ and FG-V $(\pm 70)_3$ shells are very closed, as shown in Fig. 4(b).

Fig. 5 shows the effect of temperature variation on the nonlinear-to-linear frequency ratio curves of UD and FG-X $(\pm 22)_{3T}$ and $(\pm 70)_{3T}$ shells under thermal environments $T = 300$, 400 and 500 K. The shell geometric parameter $\bar{Z} = 100$. Unlike in [25], the results from Fig. 5(a) show that the nonlinear-to-linear frequency ratio curves of UD and FG-X $(\pm 22)_{3T}$ shells are decreased as temperature rises. Like in [25], the results from Fig. 5(b) show that the nonlinear-to-linear frequency ratio curve of UD and FG-X $(\pm 70)_{3T}$ shells are increased as temperature rises. Also, the nonlinear-to-linear frequency ratio curves of the UD $(\pm 70)_{3T}$ shell are higher than those of the FG-X $(\pm 70)_{3T}$ shell.

Fig. 6 depicts the effect of shell end conditions on the nonlinear-to-linear frequency ratio curves of UD and FG-X $(\pm 22)_{3T}$ and $(\pm 70)_{3T}$ shells when $\bar{Z} = 300$ at $T = 400$ K. From Fig. 6(a), it can be found that the nonlinear-to-linear frequency ratio curve of the $(\pm 22)_{3T}$ shell is hardening type when the end condition is immovable, whereas the nonlinear-to-linear frequency ratio curve is softening type when the end condition is movable. From Fig. 6(b), it can be seen that, for UD and FG-X $(\pm 70)_{3T}$ shells, the nonlinear-to-linear frequency ratio curves are softening type for both movable and immovable end conditions when temperature variation is under consideration.

The EPR-deflection curves of $(\pm 22)_{3T}$ and $(\pm 70)_{3T}$ CNTRC laminated cylindrical shells in the large amplitude vibration region are calculated by using FEM and are plotted in Figs. 7 and 8. From Fig. 7(a), we observe that

Please cite this article as: H.-S. Shen, C. Li and J.N. Reddy, Large amplitude vibration of FG-CNTRC laminated cylindrical shells with negative Poisson's ratio, Computer Methods in Applied Mechanics and Engineering (2019) 112727, https://doi.org/10.1016/j.cma.2019.112727.

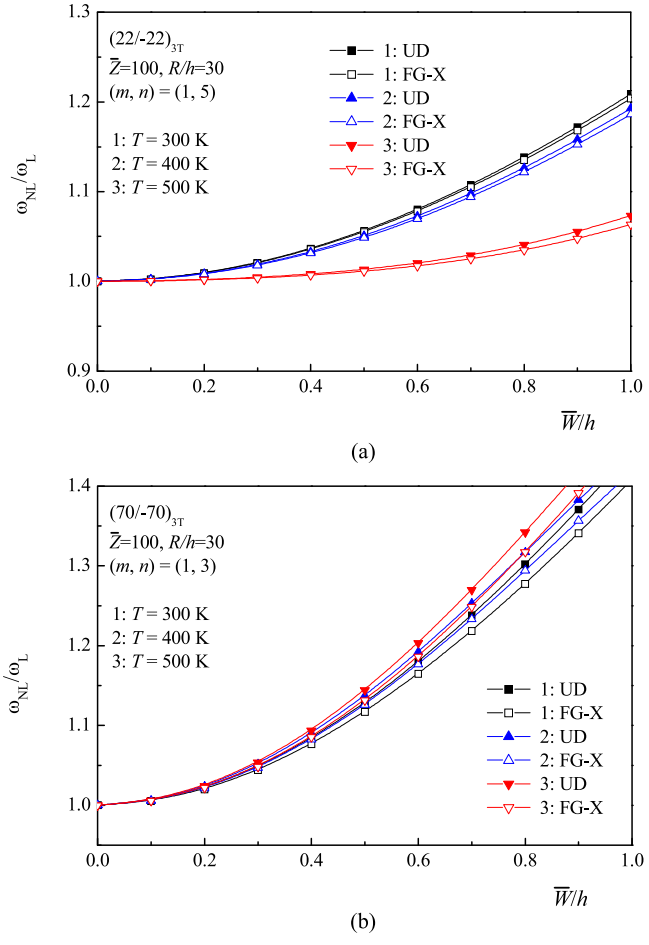

Fig. 5. Effect of temperature variations on the nonlinear vibration behaviors of CNTRC laminated cylindrical shells with negative Poisson's ratios: (a) $(\pm 22)_{3T}$ shells; (b) $(\pm 70)_{3T}$ shells.

the EPR-deflection curves of the $(\pm 22)_{3T}$ shell downward gradually when $\bar{W}/h$ becomes large. In contrast, the EPR-deflection curves of $(\pm 70)_{3T}$ shell first downward and then upward to certain values and the variation of EPR becomes smoothly when $\bar{W}/h$ is sufficiently large, as shown in Fig. 7(b). Unlike in Fig. 4(a), the FG-V $(\pm 22)_{3T}$ shell has the lowest EPR-deflection curve, while the FG-Λ $(\pm 22)_{3T}$ shell has the highest EPR-deflection curve. In contrast, the FG-Λ $(\pm 70)_{3T}$ shell has the lowest EPR-deflection curve, while the FG-V $(\pm 70)_{3T}$ shell has the highest EPR-deflection curve, as shown in Fig. 7(b). Unlike in Fig. 5(a), the EPR-deflection curves for UD and FG-X $(\pm 22)_{3T}$ shells are increased with increase in temperature, as shown in Fig. 8(a).

5. Concluding remarks

Modeling and analysis for the large amplitude vibration of functionally graded CNTRC laminated cylindrical shells with negative Poisson's ratios in thermal environments have been presented on the basis of a multi-scale approach. The volume fraction of CNT in each ply may be different, which results in a piece-wise functionally graded CNTRC shell with UD, FG-Λ, FG-V, FG-O and FG-X patterns along the thickness direction of the shell. The extended Voigt (rule of mixture) model is used for obtaining the temperature-dependent material properties of FG-CNTRC laminated cylindrical shells. The nonlinear vibration equations are solved by applying a singular perturbation technique along with a two-step perturbation approach. We found that the $(\pm 22)_{3T}$ CNT/PmPV laminated shell has the maximum NPR ν_{13}, while the $(\pm 70)_{3T}$ CNT/PmPV laminated shell has the maximum

Please cite this article as: H.-S. Shen, C. Li and J.N. Reddy, Large amplitude vibration of FG-CNTRC laminated cylindrical shells with negative Poisson's ratio, Computer Methods in Applied Mechanics and Engineering (2019) 112727, https://doi.org/10.1016/j.cma.2019.112727.

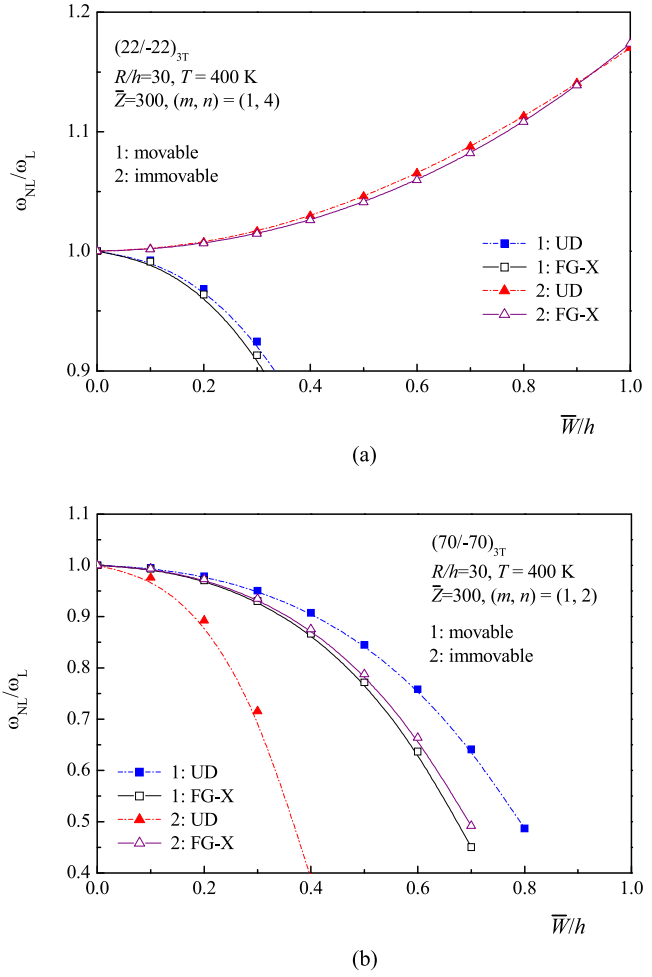

Fig. 6. Effect of shell end conditions on the nonlinear vibration behaviors of CNTRC laminated shells with negative Poisson's ratios: (a) $(\pm 22)_{3T}$ shells; (b) $(\pm 70)_{3T}$ shells.

NPR ν_{23}. The numerical results reveal that the characteristics of nonlinear vibration are significantly influenced by EPRs. The EPR-deflection curves for CNTRC laminated cylindrical shells are obtained for the first time.

Acknowledgments

This work is supported in part by the National Natural Science Foundation of China under Grant 51779138. The first and second authors are grateful for this financial support.

Appendix A

In Eqs. (11)–(14), the thermal forces, moments and higher order moments $\bar{N}^T$, $\bar{M}^T$ and $\bar{P}^T$ of the shell are evaluated by

$$\begin{bmatrix} \bar{N}_x^T & \bar{M}_x^T & \bar{P}_x^T \\ \bar{N}_y^T & \bar{M}_y^T & \bar{P}_y^T \\ \bar{N}_{xy}^T & \bar{M}_{xy}^T & \bar{P}_{xy}^T \end{bmatrix} = \sum_{k=1}^{N} \int_{h_{k-1}}^{h_k} \begin{bmatrix} A_x \\ A_y \\ A_{xy} \end{bmatrix}_k (1, Z, Z^3) \Delta T \, dZ \tag{A.1a}$$

Please cite this article as: H.-S. Shen, C. Li and J.N. Reddy, Large amplitude vibration of FG-CNTRC laminated cylindrical shells with negative Poisson's ratio, Computer Methods in Applied Mechanics and Engineering (2019) 112727, https://doi.org/10.1016/j.cma.2019.112727.

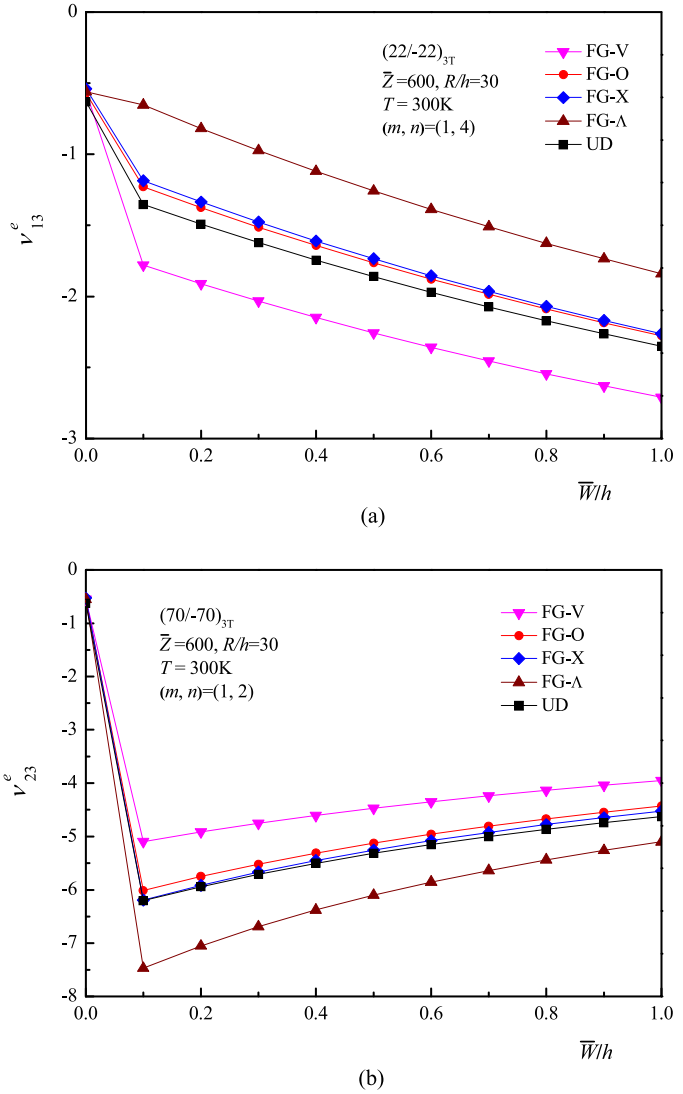

Fig. 7. EPR-deflection curves of CNTRC laminated cylindrical shells with negative Poisson's ratios: (a) $(\pm 22)_{3T}$ shells; (b) $(\pm 70)_{3T}$ shells.

and $\bar{S}^T$ are defined by

$$\begin{bmatrix} \bar{S}^T_x \\ \bar{S}^T_y \\ \bar{S}^T_{xy} \end{bmatrix} = \begin{bmatrix} \bar{M}^T_x \\ \bar{M}^T_y \\ \bar{M}^T_{xy} \end{bmatrix} - \frac{4}{3h^2} \begin{bmatrix} \bar{P}^T_x \\ \bar{P}^T_y \\ \bar{P}^T_{xy} \end{bmatrix} \tag{A.1b}$$

where $\Delta T = T - T_0$ is the temperature rise from the reference temperature T_0 at which there are no thermal strains in the shell, and

$$\begin{bmatrix} A_x \\ A_y \\ A_{xy} \end{bmatrix} = - \begin{bmatrix} \bar{Q}_{11}\bar{Q}_{12} & \bar{Q}_{16} \\ \bar{Q}_{12} & \bar{Q}_{22} & \bar{Q}_{26} \\ \bar{Q}_{16} & \bar{Q}_{26} & \bar{Q}_{66} \end{bmatrix} \begin{bmatrix} c^2 & s^2 \\ s^2 & c^2 \\ 2cs & -2cs \end{bmatrix} \begin{bmatrix} \alpha_{11} \\ \alpha_{22} \end{bmatrix} \tag{A.2}$$

Please cite this article as: H.-S. Shen, C. Li and J.N. Reddy, Large amplitude vibration of FG-CNTRC laminated cylindrical shells with negative Poisson's ratio, Computer Methods in Applied Mechanics and Engineering (2019) 112727, https://doi.org/10.1016/j.cma.2019.112727.

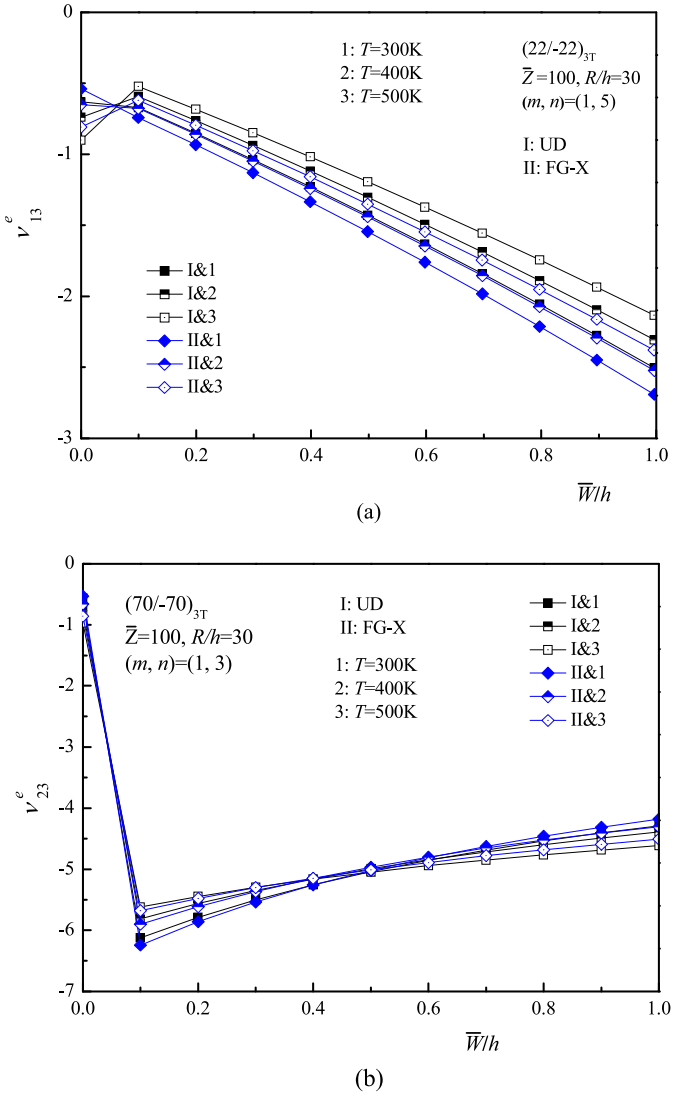

Fig. 8. Effect of temperature variations on the EPR-deflection curves of CNTRC laminated cylindrical shells with negative Poisson's ratios: (a) $(\pm 22)_{3T}$ shells; (b) $(\pm 70)_{3T}$ shells.

in which α_{11} and α_{22} are the thermal expansion coefficients for the kth ply, and $\bar{Q}_{ij}$ are the transformed elastic constants for a CNTRC layer and may be evaluated as

$$\begin{bmatrix} \bar{Q}_{11} \\ \bar{Q}_{12} \\ \bar{Q}_{22} \\ \bar{Q}_{16} \\ \bar{Q}_{26} \\ \bar{Q}_{66} \end{bmatrix} = \begin{bmatrix} c^4 & 2c^2s^2 & s^4 & 4c^2s^2 \\ c^2s^2 & c^4+s^4 & c^2s^2 & -4c^2s^2 \\ s^4 & 2c^2s^2 & c^4 & 4c^2s^2 \\ c^3s & cs^3-c^3s & -cs^3 & -2cs(c^2-s^2) \\ cs^3 & c^3s-cs^3 & -c^3s & 2cs(c^2-s^2) \\ c^2s^2 & -2c^2s^2 & c^2s^2 & (c^2-s^2)^2 \end{bmatrix} \begin{bmatrix} Q_{11} \\ Q_{12} \\ Q_{22} \\ Q_{66} \end{bmatrix} \tag{A.3a}$$

$$\begin{bmatrix} \bar{Q}_{44} \\ \bar{Q}_{45} \\ \bar{Q}_{55} \end{bmatrix} = \begin{bmatrix} c^2 & s^2 \\ -cs & cs \\ s^2 & c^2 \end{bmatrix} \begin{bmatrix} Q_{44} \\ Q_{55} \end{bmatrix} \tag{A.3b}$$

Please cite this article as: H.-S. Shen, C. Li and J.N. Reddy, Large amplitude vibration of FG-CNTRC laminated cylindrical shells with negative Poisson's ratio, Computer Methods in Applied Mechanics and Engineering (2019) 112727, https://doi.org/10.1016/j.cma.2019.112727.

where

$$Q_{11}=\frac{E_{11}}{1-\nu_{12}\nu_{21}},\qquad Q_{22}=\frac{E_{22}}{1-\nu_{12}\nu_{21}},\qquad Q_{12}=\frac{\nu_{21}E_{11}}{1-\nu_{12}\nu_{21}},$$
$$Q_{16}=Q_{26}=0,\qquad Q_{66}=G_{12},\qquad Q_{44}=G_{23},\qquad Q_{55}=G_{13} \tag{A.4}$$

where E_{11}, E_{22}, G_{12}, are the effective Young's and shear moduli and ν_{12} and ν_{21} are the Poisson's ratios of the CNTRC layer, respectively.

Appendix B

In Eqs. (19b) and (20b), the reduced stiffness matrices $[A^*_{ij}]$, $[B^*_{ij}]$, $[D^*_{ij}]$, $[E^*_{ij}]$, $[F^*_{ij}]$ and $[H^*_{ij}]$ are determined through relationships [41]

$$\mathbf{A}^*=\mathbf{A}^{-1},\qquad \mathbf{B}^*=-\mathbf{A}^{-1}\mathbf{B},\qquad \mathbf{D}^*=\mathbf{D}-\mathbf{B}\mathbf{A}^{-1}\mathbf{B},\qquad \mathbf{E}^*=-\mathbf{A}^{-1}\mathbf{E},\qquad \mathbf{F}^*=\mathbf{F}--\mathbf{E}\mathbf{A}^{-1}\mathbf{B},$$
$$\mathbf{H}^*=\mathbf{H}--\mathbf{E}\mathbf{A}^{-1}\mathbf{E} \tag{B.1}$$

where A_{ij}, B_{ij}, D_{ij}, etc., are the shell stiffnesses, defined by

$$(A_{ij},B_{ij},D_{ij},E_{ij},F_{ij},H_{ij})=\sum_{k=1}^{N}\int_{h_{k-1}}^{h_k}(\bar{Q}_{ij})_k(1,Z,Z^2,Z^3,Z^4,Z^6)dZ\quad(i,j=1,2,6) \tag{B.2a}$$

$$(A_{ij},D_{ij},F_{ij})=\sum_{k=1}^{N}\int_{h_{k-1}}^{h_k}(\bar{Q}_{ij})_k(1,Z^2,Z^4)dZ\quad(i,j=4,5) \tag{B.2b}$$

and the inertias $I_i(i=1,2,3,4,5,7)$ are defined by

$$(I_1,I_2,I_3,I_4,I_5,I_7)=\sum_{k=1}^{N}\int_{h_{k-1}}^{h_k}\rho_k(1,Z,Z^2,Z^3,Z^4,Z^6)\mathrm{d}Z \tag{B.3a}$$

in which $c_1=4/(3h^2)$ and

$$\bar{I}_1=I_1,\ \bar{I}_1'=I_1+\frac{2}{R}I_2,\ \bar{I}_2=I_2-c_1I_4,\ \bar{I}_2'=I_2+\frac{1}{R}I_3-c_1I_4-\frac{c_1}{R}I_5,\ \bar{I}_3=c_1I_4,$$
$$\bar{I}_3'=c_1I_4+\frac{c_1}{R}I_5,\ \bar{I}_4=\bar{I}_4'=I_3-2c_1I_5+c_1^2I_7,\ \bar{I}_5=\bar{I}_5'=c_1I_5-c_1^2I_7,\ \hat{I}_3=\bar{I}_4-\frac{\bar{I}_2\bar{I}_2}{\bar{I}_1},$$
$$\hat{I}_3'=\bar{I}_4'-\frac{\bar{I}_2'\bar{I}_2'}{\bar{I}_1'},\ \hat{I}_5=\bar{I}_5-\frac{\bar{I}_2\bar{I}_3}{\bar{I}_1},\ \hat{I}_5'=\bar{I}_5'-\frac{\bar{I}_2'\bar{I}_3'}{\bar{I}_1'},\ \hat{I}_7=\frac{\bar{I}_3\bar{I}_3}{\bar{I}_1}-c_1^2I_7,\ \hat{I}_7'=\frac{\bar{I}_3'\bar{I}_3'}{\bar{I}_1'}-c_1^2I_7,$$
$$\tilde{I}_5=\hat{I}_3+\hat{I}_5,\ \tilde{I}_5'=\hat{I}_3'+\hat{I}_5',\ \tilde{I}_7=\hat{I}_7-\hat{I}_5,\ \tilde{I}_7'=\hat{I}_7'-\hat{I}_5', \tag{B.3b}$$

Appendix C

In Eqs. (41) and (42)

$$G_2=\frac{1}{2}\left[\frac{3G_{33}}{4G_{31}}-\frac{5G_{32}^2}{6G_{31}^2}\right],\qquad G_4=\frac{1}{2}\left[\frac{5G_{35}}{8G_{31}}-\frac{15G_{33}^2}{128G_{31}^2}+\frac{13G_{32}^2G_{33}}{16G_{31}^3}-\frac{491G_{32}^4}{864G_{31}^4}\right], \tag{C.1}$$

for the case of simply supported boundary conditions

$$G_{30}=-\gamma_{14}\gamma_{24}\frac{m^4}{g_{210}}\frac{g_{41}g_{210}+g_{42}g_{220}}{g_{210}^2-g_{220}^2}$$
$$-\varepsilon\gamma_{14}\gamma_{24}\frac{m^2}{g_{210}}\left[\frac{(g_{31}g_{210}+g_{32}g_{220})(g_{41}g_{210}+g_{42}g_{220})+(g_{32}g_{210}+g_{31}g_{220})(g_{42}g_{210}+g_{41}g_{220})}{g_{210}(g_{210}^2-g_{220}^2)}\right.$$
$$\left.+\frac{(g_{210}^2+g_{220}^2)(g_{41}g_{310}+g_{42}g_{320})+2g_{210}g_{220}(g_{42}g_{310}+g_{41}g_{320})}{g_{210}(g_{210}^2-g_{220}^2)}\right.$$

Please cite this article as: H.-S. Shen, C. Li and J.N. Reddy, Large amplitude vibration of FG-CNTRC laminated cylindrical shells with negative Poisson's ratio, Computer Methods in Applied Mechanics and Engineering (2019) 112727, https://doi.org/10.1016/j.cma.2019.112727.

$$
\begin{aligned}
&+\frac{(g_{43}g_{210}+g_{44}g_{220})+(g_{51}g_{210}+g_{52}g_{220})}{g_{210}}\\
&-\frac{\gamma_{81}m(\Delta_{01}g_{210}+\Delta_{02}g_{220})+\gamma_{82}n\beta(\Delta_{03}g_{210}+\Delta_{04}g_{220})}{g_{00}}\Bigg]-\varepsilon^2\left([\gamma_{170}-(\gamma_{171}m^2+\gamma_{172}n^2\beta^2)]\right.\\
&-\gamma_{14}\gamma_{24}\frac{\gamma_{81}m(\Delta_{01}g_{310}+\Delta_{02}g_{320})+\gamma_{82}n\beta(\Delta_{03}g_{310}+\Delta_{04}g_{320})}{\Delta_{00}g_{210}}\\
&-\frac{\gamma_{81}m(\Delta_{05}g_{210}-\Delta_{06}g_{220})+\gamma_{82}n\beta(\Delta_{07}g_{210}-\Delta_{08}g_{220})}{\Delta_{00}g_{210}}\\
&+\gamma_{14}\gamma_{24}g_{31}\frac{g_{210}(g_{41}g_{310}+g_{42}g_{320})+g_{220}(g_{42}g_{310}+g_{41}g_{320})}{g_{210}(g_{210}^2-g_{220}^2)}\\
&+\gamma_{14}\gamma_{24}g_{32}\frac{g_{210}(g_{42}g_{310}+g_{41}g_{320})+g_{220}(g_{41}g_{310}+g_{42}g_{320})}{g_{210}(g_{210}^2-g_{220}^2)}\\
&+\gamma_{14}\gamma_{24}\frac{(g_{31}g_{51}+g_{32}g_{52})+(g_{43}g_{310}+g_{44}g_{320})}{g_{210}}+\left.\frac{g_{53}g_{210}-g_{54}g_{220}}{g_{210}}\right),
\end{aligned}
$$

$$
\begin{aligned}
&G_{31}=G_{08},\ G_{32}=\frac{1}{8}\gamma_{14}\gamma_{24}\left(\frac{m^4}{\gamma_7}+\frac{n^4\beta^4}{\gamma_6}\right)\frac{g_{210}^2-g_{220}^2}{g_{210}^2}\Phi(T),\\
&G_{33}=\frac{1}{16}\gamma_{14}\gamma_{24}\left(\frac{m^4}{\gamma_7}+\frac{n^4\beta^4}{\gamma_6}\right)\frac{g_{210}^4-g_{220}^4}{g_{210}^4}-D_{44},\\
&G_{35}=-\frac{3}{16}\gamma_{14}\gamma_{24}\left(\frac{m^4}{\gamma_7}\alpha_{613}+\frac{n^4\beta^4}{\gamma_6}\alpha_{631}\right)\frac{g_{210}^2-g_{220}^2}{g_{210}^2},
\end{aligned}
\tag{C.2}
$$

in the above equations (with other symbols are defined as in Shen [36])

$$
\begin{aligned}
&G_{08}=\gamma_{14}\gamma_{24}\frac{m^4}{g_{210}}-D_{00}+\varepsilon\gamma_{14}\gamma_{24}\frac{m^2}{g_{210}}\frac{(g_{31}g_{210}+g_{32}g_{220})+(g_{210}g_{310}+g_{220}g_{320})}{g_{210}}\\
&+\varepsilon^2\left[g_{110}+\gamma_{14}\gamma_{24}\frac{g_{310}(g_{31}g_{310}+g_{32}g_{320})+g_{320}(g_{32}g_{310}+g_{31}g_{320})}{g_{210}^2-g_{220}^2}\right]\frac{g_{210}^2-g_{220}^2}{g_{210}^2},\\
&D_{00}=\gamma_{14}(\beta^2B_{00}^{(0)}m^2+b_{00}^{(0)}n^2\beta^2)+\gamma_{14}2mn\beta^2C_{00}^{(0)}\frac{g_{220}}{g_{210}},\ D_{44}=\gamma_{14}(\beta^2B_{00}^{(4)}m^2+b_{00}^{(4)}n^2\beta^2),
\end{aligned}
\tag{C.3}
$$

and

$$
\Phi(T)=\lambda+\Theta_2(\lambda)^2+\Theta_3(\lambda)^3+\cdots
\tag{C.4}
$$

where

$$
\begin{aligned}
&\lambda=\varepsilon\frac{16}{\pi^2G_{08}}\left(\frac{1}{mn}(\gamma_{T4}m^2+\gamma_{T6}6mn\beta+\gamma_{T5}n^2\beta^2)-\varepsilon G_{03}\right)\Delta T\times\frac{h}{[D_{11}^*D_{22}^*A_{11}^*A_{22}^*]^{1/4}},\\
&G_{03}=\gamma_{14}\gamma_{24}\frac{m^2g_{01}^*}{g_{210}}+\varepsilon\gamma_{14}\gamma_{24}\frac{g_{01}^*}{g_{210}}\frac{(g_{31}g_{210}+g_{32}g_{220})}{g_{210}^2}\\
&\qquad-\varepsilon^2\frac{(g_{120}g_{210}+g_{110}g_{220})}{g_{210}}\frac{(g_{02}^*g_{210}+g_{01}^*g_{220})}{m^2g_{210}},\\
&\Theta_2=-\frac{\varepsilon^2}{16G_{08}}\gamma_{14}\gamma_{24}\left(\frac{m^4}{\gamma_7}+\frac{n^4\beta^4}{\gamma_6}\right)\frac{g_{220}}{g_{210}}\frac{g_{210}^2+3g_{220}^2}{g_{210}^2}\frac{(g_{02}^*g_{210}+g_{01}^*g_{220})}{m^2g_{210}},\\
&\Theta_3=2\Theta_2^2-\frac{1}{G_{08}}\left[\frac{1}{16}\gamma_{14}\gamma_{24}\left(\frac{m^4}{\gamma_7}+\frac{n^4\beta^4}{\gamma_6}\right)\frac{g_{210}^4-g_{220}^4}{g_{210}^4}-D_{44}\frac{g_{210}^2-g_{220}^2}{g_{210}^2}\right],
\end{aligned}
\tag{C.5}
$$

and for the case of "movable" end condition

$$
B_{00}^{(0)}=B_{00}^{(4)}=0,\qquad b_{00}^{(0)}=0,\qquad b_{00}^{(4)}=-\frac{1}{8}\gamma_{24}n^2\beta^2\frac{g_{210}^2+g_{220}^2}{g_{210}^2},\qquad C_{00}^{(0)}=C_{00}^{(4)}=0
\tag{C.6}
$$

Please cite this article as: H.-S. Shen, C. Li and J.N. Reddy, Large amplitude vibration of FG-CNTRC laminated cylindrical shells with negative Poisson's ratio, Computer Methods in Applied Mechanics and Engineering (2019) 112727, https://doi.org/10.1016/j.cma.2019.112727.

and for the case of "immovable" end condition

$$\beta^2 B_{00}^{(0)} = \varepsilon \frac{(\gamma_{24}^2\gamma_{T1} - \gamma_5\gamma_{T2}) + \frac{2\gamma_5}{\pi\gamma_{24}}(\gamma_{T2} - \gamma_5\gamma_{T1})(\vartheta b_{01}^{(5/2)} - \phi\, b_{10}^{(5/2)})\varepsilon^{1/2}}{\gamma_{24}^2 - \frac{2\gamma_5^2}{\pi\gamma_{24}}(\vartheta b_{01}^{(5/2)} - \phi\, b_{10}^{(5/2)})\varepsilon^{1/2}}\Delta T,$$

$$b_{00}^{(0)} = 0, \beta C_{00}^{(0)} = -\varepsilon\,\gamma_{T3}\Delta T, C_{00}^{(4)} = 0,$$

$$\beta^2 B_{00}^{(4)} = -\frac{1}{8}\gamma_{24}\frac{m^2 + \gamma_5 n^2\beta^2}{\gamma_{24}^2 - \gamma_5^2}\frac{g_{210}^2 + g_{220}^2}{g_{210}^2}, b_{00}^{(4)} = -\frac{1}{8}\gamma_{24}\frac{\gamma_5 m^2 + \gamma_{24}^2 n^2\beta^2}{\gamma_{24}^2 - \gamma_5^2}\frac{g_{210}^2 + g_{220}^2}{g_{210}^2}, \tag{C.7}$$

References

[1] A.A. Lakis, S. Selmane, A. Toledano, Non-linear free vibration analysis of laminated orthotropic cylindrical shells, Int. J. Mech. Sci. 40 (1998) 27–49.
[2] M.H. Toorani, A.A. Lakis, Large amplitude vibrations of anisotropic cylindrical shells, Comput. Struct. 82 (2004) 2015–2025.
[3] E.L. Jansen, A comparison of analytical–numerical models for nonlinear vibrations of cylindrical shells, Comput. Struct. 82 (2004) 2647–2658.
[4] E.L. Jansen, The effect of geometric imperfections on the vibrations of anisotropic cylindrical shells, Thin-Walled Struct. 45 (2007) 274–282.
[5] E.L. Jansen, A perturbation method for nonlinear vibrations of imperfect structures: Application to cylindrical shell vibrations, Int. J. Solids Struct. 45 (2008) 1124–1145.
[6] H.-S. Shen, Boundary layer theory for the nonlinear vibration of anisotropic laminated cylindrical shells, Compos. Struct. 97 (2013) 338–352.
[7] J.U. Surjadi, L. Gao, H. Du, X. Li, X. Xiong, N.X. Fang, Y. Lu, Mechanical metamaterials and their engineering applications, Adv. Eng. Mater. 21 (2019) 1800864.
[8] P.H. Cong, P.T. Long, N.V. Nhat, N.D. Duc, Geometrically nonlinear dynamic response of eccentrically stiffened circular cylindrical shells with negative Poisson's ratio in auxetic honeycombs core layer, Int. J. Mech. Sci. 152 (2019) 443–453.
[9] R. Zhang, H.-L. Yeh, H.-Y. Yeh, A preliminary study of negative Poisson's ratio of laminated fiber reinforced composites, J. Reinf. Plast. Compos. 17 (1998) 1651–1664.
[10] J.F. Clarke, R.A. Duckett, P.J. Hine, I.J. Hutchinson, I.M. Ward, Negative Poisson's ratios in angle-ply laminates: theory and experiment, Composites 25 (1994) 863–868.
[11] C.T. Herakovich, Composite laminates with negative through-the-thickness Poisson's ratios, J. Compos. Mater. 18 (1984) 447–455.
[12] B.M. Lempriere, Poisson's ratio in orthotropic materials, AIAA J. 6 (1968) 2226–2227.
[13] P.J. Hine, R.A. Duckett, I.M. Ward, Negative Poisson's ratios in angle-ply laminates, J. Mater. Sci. Lett. 16 (1997) 541–544.
[14] E.H. Harkati, A. Bezazi, F. Scarpa, K. Alderson, A. Alderson, Modelling the influence of the orientation and fibre reinforcement on the negative Poisson's ratio in composite laminates, Phys. Status Solidi b 244 (2007) 883–892.
[15] G.W. Milton, Composite materials with Poisson's ratios close to – 1, J. Mech. Phys. Solids 40 (1992) 1105–1137.
[16] T. Akasaka, Flexible composites, in: T.-W. Chou, F. Ko (Eds.), Textile Structural Composites, Elsevier Science Publishers, 1989, pp. 279–330.
[17] K.E. Evans, J.P. Donoghue, K.L. Alderson, The design, matching and manufacture of auxetic carbon fibre laminates, J. Compos. Mater. 38 (2004) 95–105.
[18] H.-S. Shen, Functionally Graded Materials Nonlinear Analysis of Plates and Shells, CRC Press, Boca Raton, 2009.
[19] H.-S. Shen, Nonlinear vibration of shear deformable FGM cylindrical shells surrounded by an elastic medium, Compos. Struct. 94 (2012) 1144–1154.
[20] N.D. Duc, Nonlinear Static and Dynamic Stability of Functionally Graded Plates and Shells, Vietnam National University Press, Hanoi, 2014.
[21] A.H. Sofiyev, Large amplitude vibration of FGM orthotropic cylindrical shells interacting with the nonlinear Winkler elastic foundation, Composites B 98 (2016) 141–150.
[22] A.H. Sofiyev, D. Hui, V.C. Haciyev, H. Erdem, G.Q. Yuan, E. Schnack, V. Guldal, The nonlinear vibration of orthotropic functionally graded cylindrical shells surrounded by an elastic foundation within first order shear deformation theory, Composites B 116 (2017) 170–185.
[23] N.D. Duc, P.T. Thang, Nonlinear dynamic response and vibration of shear deformable imperfect eccentrically stiffened S-FGM circular cylindrical shells surrounded on elastic foundations, Aerosp. Sci. Technol. 40 (2015) 115–127.
[24] H.-S. Shen, Nonlinear bending of functionally graded carbon nanotube-reinforced composite plates in thermal environments, Compos. Struct. 91 (2009) 9–19.
[25] H.-S. Shen, Y. Xiang, Nonlinear vibration of nanotube-reinforced composite cylindrical shells in thermal environments, Comput. Methods Appl. Mech. Engrg. 213–216 (2012) 196–205.
[26] S.M. Hosseini, Application of a hybrid mesh-free method based on generalized finite difference (GFD) method for natural frequency analysis of functionally graded nanocomposite cylinders reinforced by carbon nanotubes, CMES Comput. Model. Eng. Sci. 95 (2013) 1–29.
[27] A. Alibeigloo, H. Jafarian, Three-dimensional static and free vibration analysis of carbon nanotube reinforced composite cylindrical shell using differential quadrature method, Int. J. Appl. Mech. 8 (2016) 1650033.

Please cite this article as: H.-S. Shen, C. Li and J.N. Reddy, Large amplitude vibration of FG-CNTRC laminated cylindrical shells with negative Poisson's ratio, Computer Methods in Applied Mechanics and Engineering (2019) 112727, https://doi.org/10.1016/j.cma.2019.112727.

[28] Z.G. Song, L.W. Zhang, K.M. Liew, Vibration analysis of CNT-reinforced functionally graded composite cylindrical shells in thermal environments, Int. J. Mech. Sci. 115 (2016) 339–347.
[29] B. Thomas, T. Roy, Vibration and damping analysis of functionally graded carbon nanotubes reinforced hybrid composite shell structures, J. Vib. Control 23 (2017) 1711–1738.
[30] S. Zghal, A. Frikha, F. Dammak, Free vibration analysis of carbon nanotube-reinforced functionally graded composite shell structures, Appl. Math. Model. 53 (2018) 132–155.
[31] N. Van Thanh, V.D. Quang, N.D. Khoa, S.-E. Kim, N.D. Duc, Nonlinear dynamic response and vibration of FG CNTRC shear deformable circular cylindrical shell with temperature-dependent material properties and surrounded on elastic foundations, J. Sandwich Struct. Mater. 21 (2019) 2456–2483.
[32] P.M. Ajayan, O. Stephan, C. Colliex, D. Trauth, Aligned carbon nanotube arrays formed by cutting a polymer resin—Nanotube composite, Science 265 (1994) 1212–1214.
[33] Y. Han, J. Elliott, Molecular dynamics simulations of the elastic properties of polymer/carbon nanotube composites, Comput. Mater. Sci. 39 (2007) 315–323.
[34] R.A. Schapery, Thermal expansion coefficients of composite materials based on energy principles, J. Compos. Mater. 2 (1968) 380–404.
[35] J.N. Reddy, C.F. Liu, A higher-order shear deformation theory of laminated elastic shells, Internat. J. Engrg. Sci. 23 (1985) 319–330.
[36] H.-S. Shen, A Two-Step Perturbation Method in Nonlinear Analysis of Beams, Plates and Shells, John Wiley & Sons Inc, 2013.
[37] C.-L. Zhang, H.-S. Shen, Temperature-dependent elastic properties of single-walled carbon nanotubes: Prediction from molecular dynamics simulation, Appl. Phys. Lett. 89 (2006) 081904.
[38] P. Malekzadeh, M. Farid, P. Zahedinejad, A three-dimensional layerwise-differential quadrature free vibration analysis of laminated cylindrical shells, Int. J. Press. Vessels Pip. 85 (2008) 450–458.
[39] R. Ansari, J. Torabi, M. Faghih Shojaei, Free vibration analysis of embedded functionally graded carbon nanotube-reinforced composite conical/cylindrical shells and annular plates using a numerical approach, J. Vib. Control 24 (2018) 1123–1144.
[40] J.L. Nowinski, Nonlinear transverse vibrations of orthotropic cylindrical shells, AIAA J. 1 (1963) 617–620.
[41] H.-S. Shen, Kármán-type equations for a higher-order shear deformation plate theory and its use in the thermal postbuckling analysis, Appl. Math. Mech. 18 (1997) 1137–1152.

Please cite this article as: H.-S. Shen, C. Li and J.N. Reddy, Large amplitude vibration of FG-CNTRC laminated cylindrical shells with negative Poisson's ratio, Computer Methods in Applied Mechanics and Engineering (2019) 112727, https://doi.org/10.1016/j.cma.2019.112727.